arXiv:1609.02215v1 [astro-ph.SR] 7 Sep 2016

A Trip to the Cataclysmic Binary Zoo: Detailed Follow-Up of 35 Recently-Discovered Systems

John R. Thorstensen, Erek H. Alper, and Kathryn E. Weil

Department of Physics and Astronomy
6127 Wilder Laboratory, Dartmouth College
Hanover, NH 03755-3528

ABSTRACT

We report follow-up studies of 35 recently-discovered cataclysmic variables (CVs), 32 of which were found in large, automated synoptic sky surveys. The objects were selected for observational tractability. For 34 of the objects we present mean spectra and spectroscopic orbital periods, and for one more we give an eclipse-based period. Thirty-two of the period determinations are new, and three of these refine published estimates based on superhump periods. The remaining three of our determinations confirm previously published periods. Twenty of the stars are confirmed or suspected dwarf novae with periods shorter than 3 hours, but we also find three apparent polars (AM Her stars), and six systems with $P > 5$ h, five of which have secondary stars visible in their spectra, from which we estimate distances when possible. The orbital period distribution of this sample is very similar to that of previously discovered CVs.

Subject headings: keywords: stars

1. Introduction

Cataclysmic variable stars (CVs) are a broad class of binaries that include a white dwarf primary star accreting via Roche lobe overflow from a close companion, which usually resembles a cool main-sequence star; Warner (1995) gives a useful introduction.

CVs are compact, low-luminosity systems with typical orbital periods $P_{\rm orb}$ of only a few hours. Their evolution is driven largely by angular momentum loss, which over most of a CV's lifetime causes the orbit to gradually shrink. However, at a period near 75 min, the slope of the secondary's mass-radius relation reverses (at least for hydrogen-burning secondaries) which causes the orbital period to increase as angular momentum is lost.

Single white dwarfs evolve from red giants, which attain radii much larger than typical CV systems. Unless a white dwarf is formed elsewhere and later captured – an unlikely event in the field – a CV must therefore have passed through common-envelope evolution at some point, during which the secondary was engulfed by the primary, leading to rapid loss of angular momentum. Modeling

the common-envelope stage with *a priori* physics is extremely difficult, so the usual practice is to use simple parameterizations to describe the process, and match model outputs to the observed population (see, e.g., Goliasch & Nelson 2015).

Constraining the calculations requires an accurate accounting of the CV population. CVs are rather rare, low-luminosity systems, so this requires consideration of the channels through which they are discovered.

The first CVs were discovered because they were variable stars, most conspicuously classical novae, driven by thermonuclear explosions of hydrogen-rich material accreted onto the white dwarf, and also dwarf novae, in which the accretion disk around the white dwarf transitions from time to time into a much brighter state. Other CVs with less dramatic variability were found by color selection, especially ultraviolet excesses. The Palomar-Green survey found a sizable number of CVs (Green et al. 1982; Ringwald 1993), and more recently the Sloan Digital Sky Survey (SDSS) obtained spectra of 285 color-selected CVs and CV candidates, most of which were new discoveries (see Szkody et al. 2011 and previous papers in that series). Finally, many CVs emit X-rays; X-ray surveys especially tend to find CVs in which the white-dwarf primary is strongly magnetized (see, e.g., Thorstensen & Halpern 2013; Halpern & Thorstensen 2015).

In recent years several synoptic sky surveys have generated a torrent of new CV discoveries. The Catalina Real Time Transient Surveys (CRTS; Drake et al. 2009; Breedt et al. 2014; Drake et al. 2014b) have discovered over 1000 CVs on the basis of variability, most of them being discovered by the Catalina telescope and denoted as "CSS". The Russian MASTER project (Lipunov et al. 2010) has also produced a large number of new discoveries, and most recently the ASAS-SN project (Shappee et al. 2014b), has come into its own. ASAS-SN uses 14-cm aperture lenses and reaches a limiting magnitude of only ~ 16, but is now covering $\sim 20,000$ square degrees per night under favorable conditions (K. Stanek, private communication). Many transient sources fade back to magnitudes beyond the reach of spectroscopic followup on 2-m class telescopes, but a substantial minority remain tractable. ASAS-SN's fast cadence and relatively shallow limiting magnitude make it an especially rich source of CVs amenable to further study.

CVs also continue to be discovered through color selection. As examples, Carter et al. (2013) searched the SDSS for AM CVn stars (ultra-short period CVs in which both components are degenerate dwarfs), and Kepler et al. (2016) searched for hot white dwarfs and turned up twelve CVs as a byproduct.

To place the many newly-discovered CVs in context, it is necessary to follow them up, in particular to find orbital periods. Periods can often be found from photometry, but in non-eclipsing systems radial-velocity spectroscopy gives more definitive results. Spectroscopy also provides a wealth of ancillary information. We present here follow-up observations, mostly spectroscopic, of 35 newly-discovered CVs, 32 of which were found by CRTS, ASAS-SN, and/or MASTER. For all, we determine orbital periods. Thirty-two of the 35 periods are apparently are not published elsewhere, though superhump periods were available for three of of the objects. For three other

objects we confirm periods that have appeared in the literature.

The objects studied here were selected mostly on the basis of their observational tractability, and the lack of a published orbital period (although in three cases we became aware of published periods before submitting this paper). We mostly avoided systems with known superhump periods, since their orbital periods can be deduced fairly well from this information (see e.g. Gänsicke et al. 2009). JRT maintains a master list of CVs and updates it regularly with new discoveries from the ASAS-SN, MASTER, and CSS lists, and other discoveries as they come to his attention. Before every observing run, this list is searched and targets that might yield useful spectra – in practice, targets that are $\sim$ 19.5 mag or brighter at minimum – are culled out. Final selection is made at the telescope using quick-look spectra and radial velocities measured in real time. In practice, the selection process favored objects with strong Hα emission, and disfavored objects with strong continua and weak emission such as dwarf novae in outburst and some novalike variables.

2. Observations and Reductions

All our observations are from MDM Observatory on Kitt Peak, Arizona.

Spectroscopy. For nearly all the spectra, we used the 'modspec' spectrograph[1] with a 600 line mm^{-1} grating. We mostly used a SITe 2048^2 CCD detector, which yielded 2 Å pixel^{-1} from 4210 to 7500 Å, with declining throughput toward the ends of the spectral range. When this detector was unavailable, we used a very similar 1024^2 SITe detector ('Templeton'), which covered from 4660 to 6730 Å. The modspec was mounted mostly on the 2.4 m Hiltner telescope, but for some of the brighter objects we used the 1.3 m McGraw-Hill telescope. For a few of the 1.3-m spectra we used the Mark III grism spectrograph, which covered 4580 to 6850 Å at 2.3 Å pixel^{-1}. On both telescopes, and with both spectrographs, we used an Andor Ikon camera to view the reflective slit jaws through a microscope, and guided the telescope with a separate off-axis guider. With this arrangement we could place any object that was bright enough for a usable spectrum in the slit, and track it accurately even if the portion of the light spilling onto the slit jaws was invisible.

Observations from a single site must be taken at intervals of about one sidereal day, which inevitably leads to some uncertainty in the number of cycles that elapsed when the object was out of view. To minimize this uncertainy, one must take observations far from the meridian. A spectrograph slit that is oriented north-south – the default for these instruments – will then have a position angle far from the parallactic angle, along which atmospheric dispersion acts (Filippenko 1982). The resultant wavelength-dependent decentering causes light loss that varies with wavelength, and small spurious velocity shifts as well. To avoid this, at the 2.4m we rotated the instrument to align the 1.1-arcsec slit with the parallactic angle when observing at large hour angles. At the 1.3 m, the effect is less critical because of the larger projected slit width (2 arcsec) and the rotation

[1]A description of the modspec can be found at `http://mdm.kpno.noao.edu/Manuals/ModSpec/modspec_man.html`.

adjustment is much more awkward, so we did not rotate the instrument.

We derived the wavelength calibration from Hg, Ne, and Xe lamp spectra taken near the zenith in twilight. With modspec, we did not take lamps when the sun was more than 12 degrees below the horizon, and instead used the λ5577 night sky line to track and correct for drift in the zero point of the calibration. Other night-sky features that were not used in the calibration typically had mean velocities < 10 km s^{-1} and an RMS scatter of ~ 3 km s^{-1}. The night-sky technique did not give good results for the Mark III spectrograph, so with that instrument we took lamp spectra at each new telescope position, and at intervals of ~ 1 hr when following a target.

Radial Velocities. Our emission-line radial velocities are almost entirely of Hα, since it almost always gives the best signal-to-noise ratio with our instrument. We use an algorithm developed by Schneider & Young (1980), in which the line profile is convolved with an antisymmetric function and the zero of the convolution – which occurs when the positive contribution from one side of the line balances the negative contribution from the other side – is taken as the line center. When measuring the doubled, steep-sided lines of edge-on dwarf novae, we adjusted the convolution function to be sensitive to the steep sides of the line. For narrower emission lines the function we used was the derivative of a gaussian, with the width tuned to the line. To calculate uncertainties in the velocities we propagated the estimated photon-statistics uncertainties of the spectrum points through the measurement process; this will be optimistic, since it does not include any systematic effects (e.g., line-profile variations).

When a late-type secondary star was present, we found its velocity using the `xcsao` task from the `rvsao` package (Kurtz & Mink 1998), which implements the cross-correlation velocity algorithm described by Tonry & Davis (1979). As a template, we used a composite of a large number of K-type spectral standards, shifted to zero velocity, This matched the $\sim$ K-type secondaries reasonably well. The algorithm estimates uncertainties using the asymmetry in the cross-correlation.

To search for radial-velocity periods, we constructed a grid of trial frequencies with spacing Δf sufficiently dense for the time interval T covered (in practice, $\Delta f = 1/(12T)$ for long time-span searches, and denser for shorter spans). We then fit least-squares sinusoids of the form $v(t) = A\cos\omega t + B\sin\omega t + C$ at each trial frequency $\omega = 2\pi f$, and computed

$$\chi^2 = \sum_i \frac{[o_i - v(t_i)]^2}{\sigma_i^2}, \tag{1}$$

where o_i is the i-th observed data point. We display $1/\chi^2$, which is visually analogous to a periodogram, and which tends to emphasize frequencies with very low χ^2 (and hence very good fits). To test the reliability of the choice of cycle count, we used the Monte Carlo tests described by Thorstensen & Freed (1985), and in nearly all cases continued taking measurements until the likelihood of an incorrect choice was very small.

All these techniques are incorporated in a quick-look reduction pipeline for use at the telescope. With this we monitor velocities in real time, update the period search, and plan observations for

maximum period discrimination.

Photometry. For nearly all our time-series differential photometry, we used an Andor Ikon camera (the same model used for slit viewing), attached to the 1.3 m McGraw-Hill telescope at MDM. All observations were taken either unfiltered, or with a GG420 filter to suppress moonlight. The 2015 March observations of ASAS-SN 15aa, and the 2016 March observations of ASAS-SN 15cw, were taken through the slit-viewing microscope, with the target well away from the slit. These images were cosmetically poor but proved adequate for eclipse timing. The rest of the data were taken with the camera in direct imaging mode. Exposures were typically 10-30 sec, with almost no dead time. We subtracted bias and dark frames from the raw images, and divided by a flat field image taken in twilight.

To measure instrumental magnitudes we used the IRAF `phot` routine, with for the most part a 3-arcsec radius aperture. In each image we measured the program star, a brighter comparison star, and at least one check star. Because of our non-standard passband we did not observe photometric standard stars. We instead used catalog data to find or estimate V magnitudes for the comparison stars, and added these to the differential magnitudes to align them very roughly with V.

Secondary star contributions and distances. Several objects show a late-type contribution due to a secondary star. When this was sufficiently distinct, we estimated its spectral type and contribution in the following manner. First, if the secondary's radial velocities were measurable, we shifted the individual spectra into the rest frame of the secondary and co-added them. We then scaled and subtracted spectra of stars from a range of spectral type, and adjusted the type and scale factor to best cancel the late-type features. The spectral type and estimated flux contribution correlate strongly, since metal features tend to grow stronger toward cooler types.

To estimate distances using the secondary contributions, we used a Monte Carlo technique described in Thorstensen & Halpern (2013). Briefly, we use the orbital period and a rough estimate of the secondary's mass to constrain its radius (which depends only weakly on the mass), and then use its spectral type to estimate its surface brightness; combining these with its flux contribution then yields a distance. Note that we do not assume that the secondary follows a main-sequence mass-radius-temperature relation. The Monte Carlo technique picks all the input quantities from assumed distributions, and in particular accounts for the correlation between spectral type and secondary star contribution.

3. The Individual Stars

Table 1 lists the objects, their coordinates, and the shorter names we use here, in order of right ascension.

Figures 1 – 9 show velocities, velocity periodograms, and folded velocities for 33 of the objects discussed here. Table 2 lists all the radial velocities, and Table 3 gives parameters of sinusoidal fits

to the velocities. Table 4 gives eclipse timings for the four objects in which we observed eclipses.

3.1. CSS0015+26

The CRTS alert on this source identified it with the ROSAT X-ray source 1RXS J001538.2 +263656 (Drake et al. 2014b). The CRTS DR2 light curve shows a quiescent magnitude near 18 mag for this dwarf nova, with three outbursts to $\sim$ 14 mag between 2005 and 2013, the brightest outburst reaching 13.3. Szkody et al. (2014) obtained eight spectra in the blue, and suggested a period near 100 min.

Our mean spectrum (Fig. 1) shows strong emission on a blue continuum, similar to that published by Szkody et al. (2014) but covering a greater spectral range. Hα has an equivalent width (EW[2]) of 80 Å, and a full width at half-maximum (FWHM) of 1200 km s^{-1}. The He II emission line is present, but much weaker than Hβ. The synthesized V is 17.7, consistent with minimum light.

We first observed this object in 2012 September, but obtained only fragmentary data before the object went into outburst on the night of 2012 Sep. 9 UT[3]. We obtained more extensive data in quiescence in 2014 October, which are best fit by $P_{\rm orb} = 2.436(2)$ hr, toward the lower end of the period gap but well inside it. Although dwarf novae in the gap are somewhat unusual, the period is reasonably secure, since the data span over 7 hr of hour angle. The adopted period results in much better fits to the data than alternate choices of cycle count.

There seems to be no record in the literature of superhumps appearing in this star. Vsnet-alert 13818[4] describes the 2009 outburst as having "quickly faded", and the 2012 outburst appears to have also faded rapidly; a superoutburst may not have occurred.

3.2. ASAS-SN 14dr

This dwarf nova was detected by ASAS-SN on 2014 July 8, reaching $V \sim 15$. In the CRTS light curve it is typically $V \sim 18.5$ in quiescence, with variation by over a magnitude, and there

[2]We quote emission-line equivalent widths as positive.

[3]The CRTS light curve missed this outburst. The next CRTS measurement, taken seven days later, showed the source at 17.1 mag.

[4]Vsnet-alert is an email service to alert observers to interesting targets; an explanatory page is found at `http://ooruri.kusastro.kyoto-u.ac.jp/mailman/listinfo/vsnet-alert`, which links to monthly archives of past alerts. Many archived alerts were posted by T. Kato of Kyoto University. Archived alerts are challenging to reference in the traditional format, since they are not indexed at ADS, SIMBAD, or other sites. We adopt the practice of citing these by number, and where possible mentioning the observers who contributed. We only cite vsnet when it provides information that we have been unable to find elsewhere.

are two previous outbursts.

The summed spectrum (Fig. 1) shows a blue continuum with strong emission lines typical of a dwarf nova at minimum light. The synthesized $V \sim 19.2$, and Hα has a FWHM near 1800 km s^{-1} and an emission EW of 140 Å. The line is double-peaked, with the peaks separated by ~ 600 km s^{-1}. The velocity period, 95.83(13) min, is determined without significant ambiguity. At this period, we can anticipate the appearance of superhumps in a future outburst.

3.3. CSS0133+38

Drake et al. (2014b) identify this dwarf nova with the ROSAT X-ray source 1RXS J013308.9 +383218. The average spectrum (Fig. 1) shows strong, single-peaked emission lines; the EW of Hα is 220 Å, and its FWHM is 1150 km s^{-1}. The synthesized V magnitude is 18.9. The CRTS DR2 light curve shows a typical quiescent magnitude near 18.5, with occasional excursions as faint as nearly 20th magnitude, and a single outburst up to 16.0 in late 2009; vsnet-alert 17667 reported a second outburst in 2014 August, but it faded rapidly. The radial velocities indicate $P_{\rm orb} = 108.0(2)$ minutes, without significant ambiguity. At this period, superhumps are to be expected if a superoutburst occurs.

3.4. CSS0143+26

This dwarf nova is apparently detected in the ROSAT Faint Source Survey as 1RXS J014306.4 +263834. The spectrum (Fig. 1) appears typical for a dwarf nova at minimum light; Hα has an EW of 75 Å and a FWHM of almost 1200 km s^{-1}, and the V magnitude synthesized from the spectrum is 18.1. The CRTS light curve shows a typical quiescent magnitude near 17.5, with at least a half-magnitude of scatter around this, and a single unambiguous outburst in 2006 December that reached 14.9 mag. The radial velocities indicate $P_{\rm orb} = 92.4(3)$ min, a range in which superhumps can be expected.

3.5. OT0150+37

Lazavera et al. (2013) discovered this CV in data from the MASTER robotic telescope network, and identified it with the faint ROSAT X-ray source RXS J015017.0+375614. The CRTS light curve appears unusual, with irregular variations between 17th and 19th magnitude and occasional outbursts to brighter than 15th. Denisenko (2013; Vsnet-alert 16457) monitored the source more closely and suggested that it might be an active polar, or AM Her star. Szkody et al. (2014) obtained spectroscopy on one night, indicating an orbital period near 103 min, which was corroborated by two humps seen in 2.8 hours of time series photometry. Because the HeII λ4686 line was absent,

and the velocity amplitude modest, they rejected the polar classification.

The mean MDM spectrum from 2013 October (Fig. 2) appears normal for a dwarf nova, in agreement with the conclusions of Szkody et al. (2014). HeII λ4686 does appear weakly, with an equivalent width of ~ 5 Å. The source was in its intermediate state, with a synthesized $V = 16.7$. The single-peaked Hα emission line had an EW of 60 Å and a FWHM near 1000 km s^{-1}. The radial velocities clearly indicate $P_{\rm orb} = 213.3(4)$ min, or 3.555(7) hr. Because the present data are much more extensive than those of Szkody et al. (2014), and have a much greater hour-angle span, this period supersedes their 103-min period. The two bumps seen in their photometry may arise from random variation rather than representing a sustained periodic modulation; more extensive time-series photometry would be needed to decide this.

The previous month we had obtained two spectra on 2013 Sept. 11 UT, and a single spectrum on Sept. 15. The latter showed the source in outburst, with weak Balmer emission on a strong blue continuum, and a synthesized V magnitude of 15.4. None of our spectra were taken in the 19th-magnitude deep low state.

The outburst spectrum and weakness of HeII λ4686 both support a dwarf nova classification. However, the light curve renders the classification somewhat tentative.

3.6. CSS0208+37

This CV was discovered on 2010 December 7, and lies 28 arcsec from 1RXS J020802.6+373236. Thorstensen & Skinner (2012) obtained a spectrum, but no time-series observations. The CRTS light curve shows a fairly steady quiescent magnitude near 17.8, with outbursts in 2006, 2008, and 2010.

Vsnet-alert 12467 reports detection of a 0.45 mag oscillation with a a period of only 0.0193 d, or 27.8 min, and credits the detection to Maksim Andreev of the Terskol team. If such a short period were orbital it would suggest a double-degenerate CV, or AM CVn star, but the spectrum (Fig. 2), which appears similar to that shown by Thorstensen & Skinner (2012), but with better signal-to-noise, has normal Balmer emission lines and resembles the spectrum of an ordinary dwarf nova. Hα has an EW of ~ 80 Å, a FWHM of 2000 km s^{-1}, and a double-peaked profile with peak separation ~ 825 km s^{-1}.

We have observations from several observing runs, the most extensive being 2013 January. The Hα radial velocities define an unambiguous period near 84.2(2) min, consistent with expectations from the spectrum. The spectroscopy and the light curve are both consistent with a normal short-period dwarf nova. We cannot shed any light on the 27.8-min photometric oscillation.

3.7. ASAS-SN 14dx

This transient was detected by ASAS-SN on 2014 July 12; they noted that it corresponds to a GALEX and XMM-Newton source. Kaur et al. (2014) obtained spectra in late August; their description is consistent with the 2014 October spectra presented here (Fig. 2). The CRTS DR2 data show the target as consistently near 16.2 mag, with one detection at 16.6. In vsnet-alert 18017, T. Kato reports that Josch Hambsch and Berto Monard detect a persistent photometric period of 0.05750 d; Kato was able to tie this to the long-term CRTS light curve and refine the photometric period to 0.0575060(2) d, or 82.8086(3) min.

The mean spectrum shows a strong, blue continuum with double-peaked emission lines. The Hβ and Hγ lines (the latter near the end of the spectral range) are flanked by absorption, very likely contributed by the white dwarf. The continuum appears 'wavy', but the 'waviness' is unlikely to be real, because the modular spectrograph is known to sometimes produce irreproducible waves in continua, which we are unable to calibrate out. The EW of Hα is 95 Å, its FWHM is 1400 km s^{-1}, and its double peaks are separated by a bit more than 500 km s^{-1}. The Hα radial velocities are modulated at an unambiguously-defined period of 82.88(8) min, consistent with the more accurate photometric period, and confirming that the photometric signal is orbital in nature.

It is unusual to discover a new dwarf nova with such a bright minimum magnitude. The URAT1 astrometric catalog (Zacharias et al. 2015) gives a proper motion $[\mu_X, \mu_Y] = [+83(7), -37(7)]$ mas yr^{-1}, derived from the difference between the URAT1 and 2MASS positions. At 100 pc, this corresponds to a transverse velocity of 43 km s^{-1}, which suggests a distance less than a few hundred parsecs. The star is listed in SDSS DR12 with $g = 16.31$, $u-g = 0.13$, $g-i = -0.26$, $r-i = -0.200$, and $i - z = -0.058$.

3.8. CSS0357+10

Schwope & Thinius (2012) reported photometry and archival X-ray observations of this source, and suggested it as a candidate polar, or AM Her star. They used archival CSS photometry to find a photometric period of 0.079181(1) d, or 114.021(1) min.

Our spectra (Fig. 2) were taken with the smaller 'Templeton' detector, so the HeII λ4686 line is near the end of our coverage, but it is nearly as strong as Hβ; such strong λ4686 is characteristic of magnetic systems. Hα has an EW of 31 Å and a FWHM of 900 km s^{-1}. The radial velocities are modulated with a large semi-amplitude $K = 320(19)$ km s^{-1} at $P = 0.07918(6)$ d, identical to the Schwope & Thinius (2012) period, but less precise due to the shorter time base. The strong HeII and large velocity amplitude strongly corroborate the suggestion by Schwope & Thinius (2012) that this is a polar.

3.9. CSS0500+13

S. Kaneko discovered this object at magnitude 12.3 on 2015 November 28 (vsnet-alert 19307), and shortly afterward CSS found it independently. Its CRTS light curve shows irregular variations from roughly 16 to 17 magnitude, with one outburst to 14.3 in 2007 December, and another measurement at 15.4 in 2008 November; outbursts are evidently rather infrequent. The CV is the likely optical counterpart of the X-ray source 1RXS J050027.7+133415. Kato (vsnet-alert 19312) noted that the SDSS colors ($g = 18.59, u - g = 0.63, g - 4 = 1.03, r - i = 1.03, i - z = 0.78$) are unusually red for a CV. The SDSS magnitudes are significantly fainter than expected given the CRTS light curve, suggesting the source was in an atypically low state when the SDSS direct images were taken.

The spectrum (Fig. 3) shows a strong contribution from a secondary star of type M3.5 ±0.5. The SDSS $r - i$ color is similar to an M2 dwarf, while $i - z$ is closer to expectations for M4 (West et al. 2008), which suggests that the shorter passband included some accretion light. The spectrum has a synthesized $V = 17.7$, whereas R. H. Lupton's transformation [5] from SDSS g and r, namely $V = g - 0.5784(g - r) - 0.0038$, yields $V = 17.99$. Hα is strongly in emission with an EW of ~ 130 Å and FWHM of $\sim$1600 km s^{-1}. The Balmer lines are double-peaked, with a separation of ~ 740 km s^{-1}.

The Hα line yields a remarkably clean modulation at $P = 3.7116(6)$ hr. We observed the object on closely-spaced observing runs in 2016 February and March, and there is no ambiguity in the cycle count over that interval. The secondary's spectral type is approximately as expected at this $P_{\rm orb}$ (Knigge 2006). From the secondary star's contribution (see Section 2) we estimate the distance to be 340 ± 80 pc.

3.10. OT0647+49

This MASTER transient was discovered in images taken 2013 March 7 (Tiurina et al. 2013). It proved to be an SU UMa-type dwarf nova; Kato et al. (2014) found superhumps at 0.067774(41) d, evolving to 0.067337(31) d. The Hα emission line (Fig. 3) is broad, with a FWHM of 2100 km s^{-1}, and double-peaked, with the peaks separated by ~ 940 km s^{-1}, indicating that the orbital inclination is not far from edge-on; its EW is ~ 60 Å.

The radial velocities select a period near 0.0655 d, or 94 min. Nearly all our data are from two runs, in 2014 January and 2014 December. Separate fits to the two runs' data yielded the same period within the errors, and the weighted average (quoted in Table 3) amounts to 94.4(2) min.

[5] See `http://www.sdss.org/dr7/algorithms/sdssUBVRITransform.html`

Taking superhump period P_1 from Kato et al. (2014) and computing the superhump period excess,

$$\epsilon = \frac{P_{\rm sh} - P_{\rm orb}}{P_{\rm orb}},$$

gives $\epsilon = 0.034$. Gänsicke et al. (2009) give a relation to predict the orbital period from the superhump period, which for the two periods quoted by Kato et al. (2014) gives 0.0660(5) and 0.0656(5) d, respectively; both predictions agree reasonably well with our measured period. This appears to be a normal SU UMa star.

3.11. ASAS-SN 14kj

Little is known about this object. The CRTS light curve is sparse, showing variation from 17 to 19 mag and no detected outbursts. ASAS-SN detected it at 14.9 mag on 2014 Nov. 17. SDSS DR12 lists it at $g = 18.44$, and our mean spectrum (Fig. 3) has a synthesized $V = 18.66$. The spectrum appears normal for a dwarf nova at minimum light; Hα has an EW of $\sim$ 80 Å and a FWHM of 1500 km s^{-1}. The period, 130.4(4) min, is determined without significant ambiguity because the observations span 7.9 h of hour angle; this period lies near the lower boundary of the roughly 2-3 hr gap in the CV period distribution. Superhumps may be expected in a future outburst.

3.12. ASAS-SN 15cw

This object was discovered by ASAS-SN on 2015 Feb. 11, and reached a magnitude of 15.9. The CRTS DR2 shows it varying irregularly between about 17th and 20th magnitude, but does not show any outbursts. Our mean spectrum (Fig. 3) has synthesized $V = 18.4$.

We took spectra in 2016 February, and quickly found signs of an eclipse, in particular a strong rotational disturbance (or Rossiter-McLaughlin effect; Rossiter 1924, McLaughlin 1924) in the Hα emission line – the line center shifts abruptly to the red as the leading (blueshifted) side of the disk is eclipsed, and then to the blue as the leading side emerges, leaving the redshifted trailing side hidden (see Fig. 3). Time-series photometry on the same run showed the eclipses to be at least two magnitudes deep and recurring with a period near 113.9 min (Fig. 10). The Hα radial velocities away from eclipse were consistent with this period, but in the interest of observing efficiency we did not obtain the extensive spectroscopy needed to establish $P_{\rm orb}$ from the velocities alone. We obtained a final eclipse timing 2016 March with the slit-viewing camera on the 1.3 m telescope; including this yields for the Barycentric Julian Date at mid-eclipse

$$\text{BJD mid} = 2457431.7674(1) + 0.0791258(4)E,$$

where E is the cycle count. We attempted to refine this using the CRTS DR2, but (oddly) could not discern the eclipse in that data set.

Although the system must be nearly edge-on, the emission lines (Fig. 3) are not notably double-peaked. Hα has an EW of 130 Å and a FWHM of 1600 km s^{-1}, so they are at least rather broad, as expected.

3.13. ASAS-SN 14ag

ASAS-SN discovered this source on 2014 March 14 at 13.5 mag. The CSS light curve shows several outbursts to nearly this brightness from a typical quiescent magnitude just fainter than 16, as well as a few points near 17th. Kato et al. (2015) found eclipses of ~ 1.5 mag depth in the CRTS data, derived an eclipse ephemeris with a period near 86.9 min, and also found superhumps with $P_{\rm sh} = 0.062059(55)$ d, or 89.37(8) min.

We have spectra from 2014 December and 2016 January. The mean spectrum from 2016 January (Fig. 4) is typical for a short-period, nearly edge-on dwarf nova near minimum light. The Hα line has an EW of 90 Å, a FWHM of 1900 km s^{-1}, and double peaks separated by about 790 km s^{-1}. The double-peaked nature of the HeI lines is more pronounced, with the line centers extending down to the continuum, or, in $\lambda\lambda$ 4471, 4921, and 5015, even below the continuum. In 2016 January we also obtained time series photometry (not shown) that yielded five eclipses.

The Hα radial velocities from 2016 January independently constrain $P_{\rm orb}$ to 0.06029(5) d; including the 2014 December data yields multiple precise periods separated by 1 cycle per 397 d. One of these precise periods agrees accurately with Kato's candidate eclipse period from the CRTS; Kato's ephemeris also predicts our 2016 January eclipses accurately, confirming his choice of period. Adopting his period and using our 2016 January eclipses to set the epoch yields, for mid-eclipse,

$$\text{BJD mid} = 2457416.7385(1) + 0.060310651(2)E$$

where E is an integer cycle count. We use this for folding the velocity data in Fig. 3. Note that the radial velocities do not decrease through their mean at eclipse phase, as would be expected if they traced the motion of the motion of the white dwarf.

Like ASAS-SN 14dr, this system is unusually bright for a newly-discovered dwarf nova, suggesting it is relatively nearby. The URAT catalog (Zacharias et al. 2015) gives its proper motion as $(\mu_X, \mu_Y) = (-54, +72)$ mas yr^{-1}, with an error of about 5 mas yr^{-1} in each coordinate. Using this information alone, and assuming a velocity distribution typical of disk stars, the procedure described by Thorstensen (2003) gives a likely distance of only $\sim 60(+40, -21)$ pc. Warner (1987) developed a method of estimating the absolute visual magnitude of a dwarf nova at maximum light. While this involves a correction for inclination, the eclipse constrains the inclination of this system to be close to edge-on. If we take the inclination to be ~ 80 degrees, and use $V = 13.5$ for maximum brightness, Warner's method gives a best distance of ~ 90 pc, also quite nearby for a newly-discovered system.

3.14. ASAS-SN 14ak

This transient was detected by ASAS-SN on 2014 April 5 at 15.4 mag. It appears to be the optical counterpart of 1RXS J095056.2−294649. The CRTS DR2 light curve is fairly well-sampled, with 260 points over eight seasons. It shows the source varying by a half-magnitude or so around a mean magnitude of ~ 17.6, with one outburst in 2009 April that reached 14.15 and another in 2010 May that reached 14.9. The mean spectrum (Fig. 4) has a synthesized $V = 18.4$. Hα has a FWHM ~ 1300 km s^{-1} and an EW of ~ 130 Å; its profile is not double-peaked, but the HeI lines show two peaks at ± 400 km s^{-1} from the line center.

Because of the southerly declination, our data span only 5.5 hr of hour angle. Nonetheless, the period is determined without significant cycle count ambiguity as 127.7(1) min (11.28 cycle d^{-1}), with a daily alias at 140.7 min (10.24 cycle d^{-1}) being much less likely. This places the system near the lower edge of the period gap, and superhumps may be expected in the event of a superoutburst.

3.15. CSS1028−16

This object is apparently the optical counterpart of 1RXS J102844.2−161253. Its CRTS DR2 light curve is somewhat unusual – it mostly stays near 17th magnitude but has many excursions to nearly 20th, and no obvious outbursts. The downward excursions are persistent and do not appear to indicate eclipses. Despite the odd variability, the mean spectrum Fig. 4) appears ordinary for a CV. The single-peaked Hα line has an EW of 75 Å and FWHM ~ 1300 km s^{-1}, again not suggesting an especially high inclination. Our spectrum has a synthesized $V \sim 18.3$, near the middle of the range of variability. There is a contribution from an M-type secondary. While this is too weak to usefully constrain the secondary's spectral type or the system's distance, it does suggest that the luminosity was not especially high during our observations. The velocity data span 7.0 hr of hour angle, and determine the period uniquely as 4.553(14) hr.

The unusual variability suggests a magnetic system, but HeII λ4686 does not appear in our mean spectrum, so CSS1028−16 is likely to be some other kind of CV, possibly a Z Cam star (a dwarf nova with bright 'standstills').

3.16. SDSS 1029+48

This object was discovered by Kepler et al. (2016) in a search for new white dwarfs in the SDSS DR12. It lies 3.5 arcsec north of a slightly brighter M-type star. The CRTS light curve, which probably includes both stars, is steady around magnitude 16.15 with a single possible brightening in 2006 to ~ 15.85. so outbursts are infrequent or possibly absent.

Our spectrum (Fig. 4) resembles the SDSS spectrum, showing emission lines with double peaks

± 500 km s^{-1} from the line center. Hβ shows weak absorption flanking the emission, which probably arises from the white dwarf photosphere. The blue continuum also suggests that the white dwarf contribution is strong. Some M-type features appear weakly toward the red, but these are almost certainly contamination from the neighboring M star, which we were unable to exclude completely.

We have spectra from two runs about 16 days apart, in 2016 January and February. The radial velocity modulation is weak, but indicates $P_{\rm orb} = 91.33(1)$ min. An alternate, but unlikely, choice of cycle count between the runs gives 91.11 min, and a still more unlikely choice of daily cycle count gives 85.87 min.

On 2016 June 11 we obtained 92 min – just one orbital period – of continuous unfiltered differential photometry with the Andor camera on the 1.3 m telescope. On all but a few of the 30 s exposures the seeing was good enough to split the target reasonably well from its neighbor. Excluding a few points taken in poor seeing, the RMS scatter of the points was 0.04 mag. The light curve was featureless at this signal-to-noise, and in particular showed no eclipses.

Fig. 11 shows a phase-averaged greyscale representation of our spectra in the region of HeI λ5876. A prominent S-wave is present, which is formed where the mass-transfer stream strikes the disk. A similar S-wave is discernible in Hα, but is less conspicuous because of the strong double-peaked emission line. Tracing the HeI S-wave by eye, and fitting it with a sinusoid, gave a semiamplitude $K_S \sim 540$ km s^{-1} and phase lagging by about 60 degrees from the fit given in Table 3.

Emission line radial velocity amplitudes are notoriously difficult to interpret. The velocity amplitude $K = 22(4)$ km s^{-1} listed in Table 3 is probably confounded by the S-wave contribution, and should not be taken to indicate the white dwarf's projected velocity amplitude K_1. However, measurements of the 'horns' of the Hα line profile suggest that K_1 is indeed rather low, probably less than ~ 30 km s^{-1}. Adopting this as an upper limit would imply $K_S/K_1 > 18$. We can use this to set an inclination-independent upper limit on the mass ratio $q = M_2/M_1$, guided by integrations of particle trajectories in the Roche potential, as follows. The S-wave comes from the impact of the mass-transfer stream on the disk. The disk radius is unknown, but it must be at least as large as the periastron distance of the mass-transfer stream, and it is likely to be significantly larger. As a rough upper limit to the S-wave's in-plane velocity, we take the Keplerian speed at the periastron the gas stream would reach if it were not to collide with the disk. The hot spot's velocity is likely to be greater than the local Keplerian speed, because it includes gas from the fast-moving stream, but the hot spot is likely to be at a significantly larger radius than the periastron, so this should be a reasonable upper limit. Using a nominal $M_1 = 0.7$ M$_\odot$, we find $K_S/K_1 = 18$ for $q \sim 0.15$, so that $q <\sim 0.15$. This is not unexpected – Patterson (1998) gives $q \sim 0.1$ for stars near this orbital period.

Since this is an upper limit, it is possible that the mass ratio is much lower, which would be significant. Late in their evolution, CVs with hydrogen-rich secondaries evolve toward a minimum period near 75 min as their secondaries lose mass; in theory, further mass transfer should increase

the secondary's radius, and increase the orbital period. CVs that have evolved past the period minimum are known as 'post-bounce' systems. They should have periods somewhat longer than the minimum and anomalously low mass ratios (Zharikov et al. 2013 give a recent tabulation of post-bounce candidates). At 91 minutes, with an evidently low mass-transfer rate and a possible low mass ratio, this system may be post-bounce.

3.17. ASAS-SN 15aa

This first entry in the ASAS-SN list for 2015 was detected on 2015 Jan. 1 around 13.8 mag, and was matched to a $g = 16.8$ quiescent source. The CRTS light curve, which extends from late 2005 to mid-2013, has 289 detections over eight seasons, and detects three previous outbursts, one of which reached 13.8 mag on 2006 July 22.

The mean spectrum from 2015 March (Fig. 5) shows a strong contribution from a late-type star. We classify this as K4.5 ($\pm$1 subclass) and estimate that it contributes about half the light in the V band. The fluxed spectra imply $V \sim 17.4 \pm 0.3$ for the secondary contribution alone, where the uncertainty reflects only the range of acceptable spectral decompositions. This estimate is probably on the faint side because of occasional cloud and losses at the spectrograph slit, so we adopt $V = 17.2$ for the secondary.

The radial velocities of the late-type star are modulated with a period near 0.3755 d, or 9.01 hr, and a sizable semiamplitude $K_{\rm abs} = 175(9)$ km s^{-1}. The emission-line velocities show greater scatter, but corroborate this period. The spectral type of the donor star is normal for this period; it is cooler than predicted by a main-sequence mass-radius relation, but similar to the secondaries of other CVs in this period range (Knigge 2006).

The CSS magnitudes (excluding outbursts) show a variation with two maxima per orbit, and unequal minima, which are clearly ellipsoidal. We used these data to refine the ephemeris as follows. First, we fixed the epoch to barycentric JD (BJD) 2457109.974(4), which is the blue-to-red crossing of the absorption line velocities. This corresponds to inferior conjunction of the secondary (i.e., the phase at which an eclipse of the white dwarf would occur for an edge-on system), and its uncertainty amounts to ~ 0.01 cycle. Then, we folded the CSS magnitudes until the deeper minimum was both reasonably sharp and coincided with the chosen epoch; Fig. 12 shows the result. Because the CSS data extend nearly 10 years earlier than the chosen epoch, the period is greatly refined to 0.375540(2) d.

We obtained most of our spectra in 2015 March, using the 1.3 m telescope remotely. The absorption-line orbit and its large amplitude were immediately apparent, and suggested the possibility of an eclipse, so we obtained time-series photometry covering a predicted eclipse interval on 2015 March 26 UT, using the slit-viewing camera in unfiltered light, as described earlier. We were rewarded by the discovery of a shallow eclipse. Another eclipse light curve was obtained three days later, and on April 10 we obtained a third light curve, again remotely, using the Andor camera in

direct mode, again without a filter. Two further eclipse light curves were obtained in 2016 January.

Fig. 13 shows the light curves. The eclipse is very shallow, ~ 0.25 mag on the ingress side, and is asymmetric, recovering only by 0.1 to 0.2 mag. in egress. The center of the eclipse occurs around phase 0.007 in the absorption line ephemeris, which is consistent with zero. Because the phase of eclipse center corresponds accurately with the inferior conjunction of the red star, it seems likely that the white dwarf and the brightest regions at the disk center are being eclipsed. The asymmetry may be due to the occultation of the 'hot spot' where the mass transfer stream strikes the outer edge of the accretion disk. For our final ephemeris, we adjusted the epoch slightly to correspond to the midpoint between the steepest portions of the ingress and the egress in the April 10 light curve, yielding for Barycentric Julian Date of the inferior conjunction of secondary

$$\text{Inf. conj.} = \text{BJD } 2457109.977(3) + 0.375540(2)E.$$

This was used to compute the phases in Figs. 5 and 13.

The emission and absorption velocity curves are perfectly antiphased, to within the uncertainty. This is a necessary, but not sufficient, condition for the emission lines to trace the motion of the white dwarf. The Hα line profile appears steady around the orbit, with two roughly equal peaks separated by ~ 750 km s^{-1}, shifting smoothly with the K-velocity, as would be expected from a symmetrical accretion disk. While the emission line velocities are not nearly accurate enough to define a precise mass ratio, their best-fit amplitude is a little less than the absorption amplitude, suggesting a mass ratio not too far below unity. The masses appear to be broadly as expected; the amplitudes are consistent with a 0.6 M$_\odot$ white dwarf and a 0.55 M$_\odot$ red star in a nearly edge-on orbit (required by the eclipse).

Using the secondary star's contribution and the Monte Carlo procedure described in Section 2, we estimate the distance to be 1140 ± 250 pc. The system is very unlikely to be closer than 500 pc or more distant than 2 kpc.

3.18. CSS1055+09

The CRTS light curve of this early CSS discovery shows irregular variation between magnitudes 17.0 and 19.5 mag, with occasional outbursts to near 14th. It was discovered also in the SDSS; Szkody et al. (2011) published a spectrum in quiescence showing emission lines with a sharp peak toward the blue, and suggested this might be from an S-wave that happened to be blueshifted at the time of exposure. Thorstensen & Skinner (2012) also published a quiescent spectrum, and noted a contribution from an M3$\pm$2 secondary.

Fig. 5 shows the mean spectrum from the present data. The M-dwarf is again present but is less prominent, probably because we caught the object in a brighter state; the synthesized V is 17.6, toward the bright end of its quiescent range. The emission lines are well-defined, the EW of Hα being 70 Å. The Hα velocities give an unambiguous $P_{\rm orb} = 3.90(0.01)$ hr. A phase-averaged

greyscale representation of the Hα line (Fig. 11) shows the orbital modulation very clearly, and reveals a slight doubling of the line. The inclination is evidently rather high; eclipses are not evident in Fig. 11, but time series photometry might reveal one.

Using both both the present mean spectrum and the data from Thorstensen & Skinner (2012), we refined the secondary's spectral type to M2.75 $\pm$ 1.25. The secondary-based distance estimate (Section 2) yielded 730 (+200, −160) pc.

3.19. CSS1211-08

The CRTS light curve of this object shows it fairly steady between 17.5 and 18.5 magnitude, except for a single outburst to 15.2 mag in 2011 February. Thorstensen & Skinner (2012) published a spectrum showing strong Balmer and HeI lines. Our mean spectrum (Fig. 5) appears similar, but with better spectral coverage and signal to noise. The Balmer lines are single-peaked; Hα has an equivalent width of 70 Å and a FWHM of about 780 km s^{-1}, indicating a low orbital inclination.

The emission-line velocities from 2016 February span almost 6.8 hours of hour angle, so the daily cycle count is reasonably secure, giving $P_{\rm orb}$ = 113.9(3) min. At this period, superoutbursts and superhumps may be expected.

3.20. SDSS 1429+00

This relatively bright CV was discovered by Carter et al. (2013) in a search for AM CVn-type binaries. The CRTS DR2 light curve shows it varying irregularly between 15.0 and 15.7 mag, with no outbursts. Our spectrum (Fig. 5) shows a strong blue continuum which approximately follows a power law, $f_\lambda \propto \lambda^{-2.4}$, and relatively weak emission lines (the EW of Hα is $\sim$ 22 Å). HeII λ4686 emission has an EW $\sim$ 3 Å, and CIII/NIII blend near λ4640 is comparable in strength. The spectrum and lack of outbursts are consistent with a novalike variable.

The radial velocities give an unambiguous period of 3.560(4) d. Fig. 14 shows phase-averaged greyscale representations of the Hα emission. The most remarkable feature is a weak, broad, high-amplitude S-wave component with a semiamplitude of $\sim$ 1000 km s^{-1}. The line core appears to be double-peaked, with the peaks at $\pm \sim$ 280 km s^{-1} from the line center. The high-amplitude feature is reminiscent of a still higher-amplitude S-wave found in V795 Herculis by Haswell et al. (1994).

3.21. ASAS-SN 15dl

This was discovered by ASAS-SN on 2015 February 16, at 15.6 magnitude. The CRTS light curve shows at least 7 outbursts since coverage began in 2005, reaching as bright as 14.2. In quiescence, the object ranges from ~ 18 to ~ 16.5 mag.

We obtained a few spectra in 2015 March with the 1.3 m and modspec, but found the source in outburst and the Hα line correspondingly weak. In 2015 April the object had returned to quiescence, so we obtained more spectra with the 1.3 m and Mark III. The average quiescent spectrum (Fig. 6) shows Balmer and HeI emission, but no HeII. Hα is single-peaked, with an equivalent width of 68 Å and a FWHM of 740 km s^{-1}. The synthesized V magnitude is 18.6, rather fainter than the CRTS light curve.

The radial velocities are fitted best with a period near 5.49 hr, but a daily cycle-count alias near 7.14 hours remains possible; the data span a relatively meager 5.1 hr of hour angle because of the object's southerly declination and the time of year. The Monte Carlo test gives a discriminatory power of 0.95 for the alias choice, and a correctness likelihood of better than 99 per cent. The choice of the shorter-period alias is also corroborated by absence of secondary-star absorption features in the average spectrum.

3.22. CSS1631+10

This system is a known SU UMa-type dwarf nova, for which Kato et al. (2010) give $P_{\rm sh} = 0.063945(24)$ d, or 92.1 min. The CRTS DR2 light curve shows significant variation in quiescence, between ~ 17 and ~ 19.5 mag, and at least 5 outbursts between early 2005 and late 2013.

The mean spectrum (Fig. 6) shows broad emission lines with incipient double peaks; the EW of Hα is 95 Å and the FWHM is around 2000 km s^{-1}. The inclination is evidently not far from edge-on, but eclipses have not been reported. Since superhumps are known, it is likely that deep eclipses would not have been missed.

The emission-line radial velocities are modulated at a period near 90.2 min, just as expected from the superhump period, for which the mean $P_{\rm sh}$-$P_{\rm orb}$ relation in Gänsicke et al. (2009) would predict 90.0 ± 0.7 min. While the daily cycle count is secure, we have velocities from two observing runs ~ 44 d apart, and the cycle count is ambiguous over that interval. Precise periods based on allowed choices of the run-to-run cycle count (which give periods within 3 standard deviations of the periods derived from the individual runs) obey

$$P_{\rm orb} = \frac{44.723(4)\ {\rm d}}{714 \pm 4},$$

where the denominator is an integer.

The spectrum, and the as-expected relation between $P_{\rm orb}$ and $P_{\rm sh}$, show this to be a typical

SU UMa-class dwarf nova.

3.23. CSS1702+55

This object was detected by CRTS on 2013 April 16. Its CRTS DR2 light curve shows variations at minimum from 18.0 to nearly 20th mag, and a single outburst to 16th magnitude corresponding to its discovery. It is apparently the optical counterpart of the ROSAT X-ray source 1RXS J170207.1+551746.

Our mean spectrum (Fig. 6) shows very strong, relatively narrow single-peaked emission lines; the EW of Hα is 180 Å, and its FWHM is 830 km s^{-1}. In part because of the strength of the lines, the radial velocities show relatively little scatter around the best-fit sinusoid at $P_{\rm orb} = 99.8(2)$ min. The radial velocity amplitude $K = 35 \pm 5$ is relatively low, which together with the relatively narrow lines suggests that the orbital inclination is fairly low. At this period, superoutbursts and superhumps are expected, but none appear to have been reported as of yet.

3.24. OT 1727+38

Denisenko et al. (2014) detected this source in outburst at $V = 14.3$ using MASTER, and noted previous outbursts detected on sky survey plates and in SDSS. The CRTS DR2 light curve shows it mostly at a rather steady minimum near 17.8 mag, with at least nine outbursts between 2005 and 2013, reaching as bright at 14.6 mag.

Our mean spectrum (Fig. 6) has a synthesized $V \sim 18.5$, and appears to have been taken in quiescence. It shows typical CV emission lines on a blue continuum, with weak absorption flanking the Hβ emission, suggesting a contribution from a white dwarf photosphere; the steadiness of the minimum magnitude also suggests a stellar contribution. The Hα emission line has a relatively modest equivalent width of 43 Å, and is slightly double-peaked, with red and blue peaks at ± 320 km s^{-1} from the line center. The FWHM of the line is ~ 1300 km s^{-1}.

The emission-line velocities indicate $P_{\rm orb} = 82.14(6)$ min. This is the shortest period in the present sample. The choice of daily cycle count is reasonably secure; the Monte Carlo test gives a discriminatory power above 90 per cent and a correctness likelihood indistinguishable from unity. Superhumps have apparently not been reported, but at this $P_{\rm orb}$ they are likely to appear in future outbursts.

3.25. ASAS-SN 15cm

This was detected by ASAS-SN on 2015 Jan. 31, at magnitude 15.77. The CRTS DR2 light curve has 369 measurements between 2005 and 2013, and a single outburst to 16.3 mag in 2006; otherwise the source varies between 18.4 and 18.9. The SDSS DR12 gives $(ugriz) = (19.94, 19.10, 18.58, 18.41, 18.35)$. SDSS also took a spectrum, which shows late-type features (in particular MgI λ5175 and NaD absorption) and weak, broad, double-peaked Hα emission. The SDSS best fit is a spectrum of type K3. Our mean spectrum (top panel of Fig. 15) appears nearly identical to the SDSS spectrum, and has nearly the same absolute flux as well. The Hα line is double-peaked, with peaks at $\pm$390 km s^{-1} from the line center, and an equivalent width of only $\sim$ 9 Å.

We were unable to measure usable emission-line velocities due to faintness of the source and the weakness of the Hα emission, but the cross-correlation technique yielded radial velocities for the late-type component. These showed a strong modulation near $P_{\rm orb} = 0.209$ d, or 5.00 hr (Fig. 15, middle panel). Differential photometry of the source with the 1.3 m telescope and Andor camera quickly revealed a strong ellipsoidal modulation (Fig. 15, bottom panel).

The ellipsoidal modulation appears in the CRTS DR2 data, unambiguously but at low signal-to-noise. The CRTS data constrain $P_{\rm orb}$ to 0.208466(2) d, which we adopt.

The spectral decomposition procedure (Section 2) constrains the spectrum to K2.5 $\pm$2.5 subclasses, in good agreement with the SDSS fit. This is much warmer than expected at $P_{\rm orb} = 5$ hr; the tabulation by Knigge (2006) shows that CVs at this period more typically have secondaries around type M3. ASAS-SN 15cm therefore joins a small club of warm-secondary CVs (see, e.g. Thorstensen 2013, Rebassa-Mansergas et al. 2014, and Thorstensen 2015).

We can constrain the orbital inclination i as follows. We modeled the ellipsoidal variation using the light-curve synthesis program described by Thorstensen & Armstrong (2005). It proved difficult to match the large amplitude of the observed ellipsoidal modulation, without artificially increasing gravity darkening and decreasing the disk contribution excessively. Therefore, i is probably close to edge-on, but it cannot be too close, because the light curve shows no sign of an eclipse of the accretion disk or white dwarf. For a mass ratio $q = M_2/M_1 = 0.1$, which is smaller than likely, the white dwarf (i.e., the center of the accretion disk) will eclipse if $i > 79$ degrees (Chanan et al. 1976). The large-amplitude ellipsoidal modulation, and the lack of eclipses, constrain the plausible range for i to be between about 70 and 79 degrees.

In this range of inclination, the observed $K_2 = 229$ km s^{-1} is consistent with white dwarf masses near 0.6 – 0.7 M$_\odot$ and $q \sim 0.6$. The mass ratio exceeds unity for white dwarf masses greater than 1 M$_\odot$. The secondary-based distance estimation (see Section 2) gives 2800 $\pm$ 400 pc. The Galactic latitude is 30.7 degrees, so the star is likely to be at least 1 kpc from the Galactic plane.

3.26. CSS1735+15

A spectrum of this object was published by Thorstensen & Skinner (2012), who found Hα in emission and noted indications of a late-type secondary contribution. Kato et al. (2013) discovered photometric modulations in outburst at periods of 0.05436 and 0.05827 d, which they found puzzling but tentatively interpreted as a negative superhump and an orbital period respectively.

We obtained time series spectroscopy in 2014 June. The mean spectrum (Fig. 7) shows a strong contribution from a star with spectral type K4 $\pm$1 subtype. Decompositions indicate that the K star contributes about 80 per cent of the V-band light; fractions between 55 and 90 per cent gave acceptable results.

The absorption-line velocities derived from cross-correlation (and excluding the NaD line, which can be confused with HeI λ5876 emission) shows a modulation at $P_{\rm orb} = 0.3534(10)$ d, or 8.48 hr, with semi-amplitude $K = 136(4)$ km s^{-1}. The Hα emission line velocities have lower signal-to-noise but have a modulation consistent with this period. The 8.48-hr period therefore represents the orbital period of the CV, and is not from some line-of-sight interloper.

If we (1) assume the absorption velocity amplitude K_2 accurately reflects the secondary center-of-mass motion (2) assume that the white dwarf mass is above 0.6 solar masses, and (3) require the mass ratio $q = M_2/M_1 < 1.$, then the orbital inclination is less than about 60 degrees. The phase of the emission velocities is offset from the absorption by 0.574 ± 0.017, while the white-dwarf velocity should be offset by a half-cycle; consequently, we think it unwise to interpret the emission line velocities as the white-dwarf motions. The Baraffe & Kolb (2000) models that best match the secondary's spectral type at this orbital period have $M_2 \sim 0.65$ M$_\odot$.

We again estimated a distance using the secondary spectrum (Section 2). Because the absolute flux measurement through the spectrograph slit is uncertain, we referred to a single V-band acquisition image from the MDM OSMOS instrument (see Thorstensen & Skinner (2012)), which was taken in partly cloudy conditions, and calibrated it using V magnitudes of ten stars in the field taken from APASS (Henden et al. 2015)[6], yielding $V = 17.9 \pm 0.1$ (estimated uncertainty). For a nominal $M_2 = 0.6 \pm 0.15$ M$_\odot$ (used only to estimate the Roche lobe size), the distance came to 1830 ± 330 pc.

While the secondary spectral type is normal for this $P_{\rm orb}$, the superhump-like modulations reported in outburst by Kato et al. (2013) are unexpected, and their interpretation is not clear. The difference between the frequencies of the two modulations bears no obvious relationship to the orbital frequency.

[6]APASS, the AAVSO Photometric All Sky Survey, is described at https://www.aavso.org/apass

3.27. OT1759+14

This transient was discovered by ASAS-SN on 2013 April 05, with $V = 14.5$, and was designated ASAS-SN 13ab (Shappee et al. 2013a). A spectrum taken soon after discovery was consistent with a dwarf nova outburst. The transient was also detected by MASTER on 2013 April 11. Its location is not covered by the CSS. The star lies 15 arcsec from the Einstein X-ray source 2E 1756.8+1451. The PPMXL catalog (Roeser et al. 2010), which includes photographic magnitudes from the USNOB catalog (Monet et al. 2003), gives $b1 = 18.57$ and $r1 = 17.16$; a crude transformation published by John Greaves[7] then gives $V = 17.8 \pm 0.5$. Our mean spectrum (Fig. 7) has a synthesized $V = 18.1$, but included some data taken in poor seeing, so we adopt $V = 17.9$ as a rough magnitude at minimum.

The mean spectrum shows a strong secondary-star contribution with a spectral type of K5.5 ± 2 subtypes. Nascent molecular bands in the continuum indicate a slightly later type than the absorption lines, which match best around K5. The secondary contributes about half the light in the V band, typically giving around $V = 18.6 \pm 0.3$ for the secondary contribution.

The radial velocity of the K star is modulated with a period of 7.16(2) hr and a semiamplitude $K = 196(14)$ km s^{-1}; the orbit is unambiguous with only 17 velocities taken over 6 nights. The best period in the Hα emission-line velocity matches the absorption period within the mutual error; we adopted the weighted average, 7.17(2) hr.

The phase at which the emission lines increase through their mean velocity is 0.51 ± 0.04 in the absorption-line ephemeris, which is consistent with the phase expected if the emission lines trace the white dwarf motion. If we take this at face value, the nominal mass ratio is $M_2/M_1 = K_1/K_2 = (72 \pm 15)/(196 \pm 14) = 0.37 \pm 0.08$, which is smaller than one might expect. We have only 17 velocities, and the reliability of emission line velocities for dynamics is questionable, but this does suggest a somewhat more massive white dwarf than usual, or an undermassive secondary. Because of this, for the Monte Carlo distance estimate we assumed a secondary mass distribution centering on 0.5 M$_\odot$, slightly lower than suggested by the Baraffe & Kolb (2000) calculations. The secondary mass enters only weakly into the calculation, which gave $d = 1600 \pm 400$ pc. Distances less than 900 pc and greater than 3 kpc are very unlikely.

3.28. DDE23

This object was discovered by Denisenko (2012) in a search for variable stars in the USNO B1.0 catalog. It lies outside the sky coverage of CSS. Nearly all our data, from 2013 June, were taken using the 1024^2 'Templeton' detector and hence cover from just short of HeII λ4686 to somewhat longward of Hα (see Fig. 7). The source was in a relatively bright state at that time (synthesized

[7]Available at http://www.aerith.net/astro/color_conversion/JG/USNO-B1.0.html

$V = 18.6$), showing strong emission lines, including HeII λ4686 over half the strength of Hβ, which usually indicates a magnetic system. We returned to the source in 2013 September, but found it much fainter and were unable to obtain further velocities.

Although the data are not extensive, the radial velocities from 2013 June define a unique period of 2.210(2) hr, with a large velocity semiamplitude $K = 318(21)$ km s^{-1}. The large K and strong HeII λ4686 strongly suggest that this is a polar, or AM Her star.

3.29. ASAS-SN 13bs

This object was discovered by ASAS-SN on 2013 August 1. It is associated with the ROSAT X-ray source 1RXS J183008.4+373636 (Haakonsen & Rutledge 2009). This part of the sky is not covered by the CSS, and its outburst history appears to be unknown.

We observed the source in 2013 September, but could not determine an unambiguous orbital period. In 2014 June we obtained spectra with better hour-angle coverage and less velocity scatter, and determined the daily cycle count without ambiguity. The correct period corresponds to the third-best alias in the September data.

The mean spectrum from 2014 June (Fig. 7) shows strong, incipiently double-peaked emission lines on a blue continuum; the 2013 September spectrum appears similar. Hα has an EW of 110 Å and a FWHM of 1600 km s^{-1}. HeII λ4686 is present but much weaker than Hβ, and HeII λ5411 is absent despite very good signal-to-noise, so the system is unlikely to be magnetic; it is apparently a dwarf nova.

Separate fits to the velocities from the two observing runs yield consistent periods with a weighted average of 82.44(11) min. At this period, superoutbursts and superhumps can be expected.

3.30. DDE14 = 1RXS J185310.0+594509

This is among the few CVs in this paper that were not discovered by a variability survey, though soon after it was first recognized it did turn up in the ASAS-SN survey. It was identified by Denisenko & Sokolovsky (2011), who found it by searching for blue and variable stars in the USNO-B catalog (Monet et al. 2003) in the vicinity of unidentified ROSAT sources. They classified the star as a CV and identified it with 1RXS J185310.0+594509. ASAS-SN detected an outburst on 2013 August 13, at $V = 15.18$. The relatively sparse CRTS light curve (67 measurements in 8 years) did not catch any outburst, mostly showing the source between 18th and 19th mag, with one point at 19.87. Kato et al. (2015) report a superhump period of 0.059521(32) d, or 85.71(5) min, confirming that this is an SU UMa star.

The spectrum (Fig. 8) shows the strong, double-peaked emission lines characteristic of a high-

inclination dwarf nova at minimum light. Hα has an EW of 90 Å and a FWHM of 2000 km s^{-1}; its two peaks are separated by 1050 km s^{-1}. The radial velocities unambiguously indicate $P_{\rm orb} = 83.89(14)$ min. This is well within the range expected from the observed superhump period (Gänsicke et al. 2009).

3.31. CSS2133+19

This is one of 18 dwarf novae found and classified by Drake et al. (2014a), as byproducts of a search for periodic variables in the CSS data. The CSS light curve shows a minimum varying from 17.0 to 17.5 mag, and at least five distinct outbursts between 2006 and 2013, reaching a maximum near 14.4 mag. Drake et al. (2014a) flagged this and three of the other CVs that were in the SDSS footprint as having a color excess suggesting a strong contribution from the companion star.

The mean spectrum (Fig. 8) shows a significant contribution from a K5 ($\pm$ about 1.5 subclass) secondary, which contributes about 40 % of the light in the V band. The magnitude is uncertain; the synthesized magnitude is $V = 17.3$, but the SDSS DR12 magnitudes and colors imply $V \sim 17.6$, and the mean CSS magnitude around minimum is $V \sim 17.2$. For purposes of estimating the distance, we take the magnitude at minimum light to be $V = 17.3 \pm 0.5$.

The radial velocities of the absorption and emission yield nearly identical periods, with a weighted average of 9.025(12) hr. The secondary's spectral type is typical for CVs near this period (Knigge 2006). The Monte Carlo procedure distance estimation procedure described in Section 2 yields a distance of 1890 (+610, −440) pc. Distances less than 1 kpc and greater than ~ 3 kpc are unlikely. At these Galactic coordinates ($l = 71$ and $b = -23.4$ degrees) and a distance of 1890 pc, the source would lie 750 pc from the Galactic plane.

3.32. CSS2156+19

We have no spectra of this object, but Szkody et al. (2014) obtained a blue spectrum which shows double-peaked Balmer emission indicating a high inclination. The CRTS listing notes an eclipse, so we obtained differential time-series photometry with the 1.3 m telescope and Andor camera on three nights in 2014 October. The light curves (Fig. 16) show an eclipse with a depth of ~ 2 mag on a period near 102 minutes, along with a strong pre-eclipse hump. At minimum light the object was near our limiting magnitude, so the eclipse depth is not measured accurately, but it appears to be at least 2 mag. Our 2014 October data constrain the period to be 0.070922(9) d. To refine this, we folded the CRTS archival data on periods near this, and examined the resulting folded light curve while gradually shifting the fold period. An apparent eclipse emerged from the data at $P = 0.0709291(1)$ (see Fig. 12). A single eclipse kindly obtained with the 1.3m telescope

in 2015 December by K. Bakowska confirms the long-term ephemeris, which is

$$\text{BJD mid} = 2456941.7307(4) + 0.0709291(1)E,$$

where E is the cycle count.

3.33. CSS2227+28

The Catalina survey discovered this object on 2009 May 31. The CRTS light curve shows only two outbursts from a typical quiescent magnitude near 18. Thorstensen & Skinner (2012) published a spectrum covering the Hα emission line, which was single-peaked with an EW of 115 Å. The present mean spectrum (Fig. 8) shows Hα even stronger, with 160 Å equivalent width and a FWHM close to 1000 km s^{-1}. The synthesized V magnitude is $\sim$ 18.6, consistent with the quiescent state. The spectrum appears typical for a quiescent dwarf nova.

The radial velocities indicate a period near 131.0(3) min, with little ambiguity in the daily cycle count. This is just at the lower edge of the so-called 2-to-3 hour gap in the CV period distribution.

3.34. CSS2319+33

This object is apparently the optical counterpart of the ROSAT X-ray source 1RXS J231909.9+331544. The CRTS light curve shows irregular variation from 16.3 to 19.5 mag between 2005 and 2014, with the bulk of the measurements between 17th and 18th magnitude. Discrete outbursts are not seen, suggesting that this is a novalike variable rather than a dwarf nova.

The mean spectrum (Fig. 8) shows strong, single-peaked emission lines. Hα has an EW of 110 Å and a FWHM of 1200 km s^{-1}. HeII λ4686 (near the edge of the spectral coverage) appears weakly, and HeII λ5411 is not apparent, so this is unlikely to be a magnetic system. The Hα radial velocity shows a clear modulation at 3.508(5) hr; cataclysmics in this period range tend to be novalike variables rather than dwarf novae. Many CVs in this period range show complex phase-dependent changes in the line profile, associated with the SW Sex phenomenon (Thorstensen et al. 1991) but this was not apparent in a phase-averaged greyscale representation of the spectra (not shown).

3.35. CSS2335+12

This source was found by the Catalina survey on 2013 December 14. Its CSS light curve shows irregular variability around a mean of roughly 19th magnitude, with excursions as bright as 17.3 mag and fainter than 19.5 mag. A single measurement in 2013 June puts it at 20.3 mag. The CSS listing notes it as a possible polar, or AM Her star.

The mean spectrum (Fig. 9) shows HeII λ4686 with a strength comparable to Hβ, as well as HeII λ5411. The lines are narrow with broad bases, which together with the high excitation support the polar classification. There is a contribution from a late-type star, which is almost certainly the secondary star. The late-type component cannot be classified to high precision – acceptable decompositions are possible from M1 to M4. The secondary's contribution gave a distance estimate (Section 2) of 1400 ± 500 pc.

We have radial velocities from two adjacent nights that define an unambiguous period of 3.884(17) hr. Fig. 11 shows a phase-averaged greyscale representation of the spectrum. The Hα line shows a sharp component with a clear velocity modulation, and a diffuse component with a greater amplitude that is offset in phase, a pattern commonly seen in polars. The sharp component is probably from the heated face of the secondary star, and the diffuse component from the accretion stream near the white dwarf. In the greyscale representation the HeII λ5411 line (not shown) shows only the diffuse, large-amplitude component, consistent with an origin in the accretion column. Although λ5411 is weaker than HeII λ4686, it is more distinct in the greyscale because of the better instrumental sensitivity at the longer wavelength.

4. Summary and Discussion

In the last column of Table 1, we give the subtype of each of the objects, and briefly note other notable characteristics. The majority of the stars were found in variability surveys, so it is not surprising that most are dwarf novae, or U Geminorum stars; a few are listed as 'UG:' because their outburst history is not known. Twenty of the known or suspected dwarf novae have $P_{\rm orb}$ shorter than ~ 3 hr, the period range in which superoutbursts and superhumps are found; however, only four of the 20 have known superhump periods.

A superhump period would be especially desirable for SDSS1029+48, which appears to be a low mass-transfer rate system, with an apparent white dwarf component in its spectrum, and broad, double-peaked lines that show little orbital motion. Its orbital period of 91 min, (a cycle-count alias is unlikely) is significantly longward of the ~ 75-min period minimum for CVs with 'normal' hydrogen-rich secondaries, so it is a candidate 'post-bounce' system. If this is the case, it should have a superhump period excess that is anomalously small for its orbital period.

While most of the sample are either dwarf novae or resemble them spectroscopically, a few are not. Three objects appear to be polars, or AM Her stars – CSS0357+10 (already classified by Schwope & Thinius 2012), DDE23, and CSS2335+12. Two others, SDSS1429+00 and CSS2319+33, appear to be novalike variables in the period range frequented by SW Sex stars.

We find eclipses in four of the objects. The most unusual of these is ASAS-SN 15aa, which has a relatively long $P_{\rm orb}$ of 9.01 hr, a large secondary-star contribution, a sizeable ellipsoidal variation, and a distinctive, asymmetric, shallow eclipse. Another, ASAS-SN 15cw, eclipses deeply on a 114-min period and shows a spectacular rotational disturbance in its emission line velocities.

In six of the stars we detect late-type secondaries well enough to classify them and estimate distances. In most of them the secondary's spectral type is as expected given $P_{\rm orb}$, but the secondary in ASAS-SN 15cm is anomalously warm for its 5.0-hr period. That system also shows a strong photometric modulation that appears to be mostly ellipsoidal.

Two objects, ASAS-SN 14dx and ASAS-SN 14ag, show significant proper motions and appear to be relatively nearby CVs that have escaped attention until their recent discovery.

Gänsicke et al. (2009) showed that the sample of CVs discovered by SDSS finally revealed the long-sought 'spike' in the period distribution just above the minimum period for hydrogen-burning CVs. It is interesting to ask whether, in an analogous fashion, the present sample might show any systematic difference from the sample of previously-known CVs.

For the period distribution, the answer to this is evidently "no". Fig. 17 shows a comparison of the cumulative distribution functions (CDFs) of the periods presented in this paper, most of which appear here for the first time, and the periods of 999 CVs and related objects with well-determined periods listed in version 7.23 of the Ritter-Kolb catalog (Ritter & Kolb 2003; hereafter RKcat). The distributions are remarkably similar, except for the small tail of very short period systems (mainly AM CVn systems) present in RKcat. Both CDFs show a predominance of systems below the 2-3 hr 'gap', and show a distinct change of slope in the gap. The present sample does have three systems with $P_{\rm orb} > 8$ hr, whereas fewer might be expected given the RKcat distribution, but the differences between the two distributions are not statistically significant by the Kolmogorov-Smirnov test.

It is interesting that so many new CVs are still being turned up. Breedt et al. (2014) argue that the Catalina survey has already discovered most of the high-accretion rate dwarf novae within its survey area. In our sample, 30 of the 35 objects were discovered by the ASAS-SN, Catalina, or MASTER surveys, and therefore have well-defined discovery dates. Of these, 5 were discovered in 2015, 8 in 2014, 6 in 2013, and 11 before that. These numbers are small, but do not show an obvious decline in the discovery rate. It may take some time before we can be confident that even the dwarf nova sample is close to complete.

5. Acknowledgements

We gratefully acknowledge support from NSF grant AST-1008217, and thank the MDM staff for observing assistance. We also thank Karolina Bakowska of the Nicolas Copernicus Astronomical Center for obtaining an observation of CSS 2156+19.

This paper uses data from the Catalina Sky Survey and Catalina Real Time Survey; the CSS is funded by the National Aeronautics and Space Administration under Grant No. NNG05GF22G issued through the Science Mission Directorate Near-Earth Objects Observations Program. The CRTS survey is supported by the U.S. National Science Foundation under grants AST-0909182. This research has made use of the APASS database, located at the AAVSO web site. Funding

for APASS has been provided by the Robert Martin Ayers Sciences Fund. This paper uses data from the Sloan Digital Sky Survey. Funding for SDSS-III has been provided by the Alfred P. Sloan Foundation, the Participating Institutions, the National Science Foundation, and the U.S. Department of Energy Office of Science. The SDSS-III web site is http://www.sdss3.org/. SDSS-III is managed by the Astrophysical Research Consortium for the Participating Institutions of the SDSS-III Collaboration.

Facilities: Hiltner, McGraw-Hill

REFERENCES

Baraffe, I., Kolb, U. 2000, MNRAS, 318, 354

Breedt, E., Gänsicke, B. T., Drake, A. J., et al. 2014, MNRAS, 443, 3174

Carter, P. J., Marsh, T. R., Steeghs, D., et al. 2013, MNRAS, 429, 2143

Chanan, G. A., Middleditch, J., & Nelson, J. E. 1976, ApJ, 208, 512

Denisenko, D. V., & Sokolovsky, K. V. 2011, Astronomy Letters, 37, 91

Denisenko, D. V. 2012, Astronomy Letters, 38, 249

Denisenko, D., Lipunov, V., Gorbovskoy, E., et al. 2014, The Astronomer's Telegram, 5724

Drake, A. J., Djorgovski, S. G., Mahabal, A., et al. 2009, ApJ, 696, 870

Drake, A. J., Graham, M. J., Djorgovski, S. G., et al. 2014, ApJS, 213, 9

Drake, A. J., Gänsicke, B. T., Djorgovski, S. G., et al. 2014, MNRAS, 441, 1186

Gänsicke, B. T., Dillon, M., Southworth, J., et al. 2009, MNRAS, 397, 2170

Filippenko, A. V. 1982, PASP, 94, 715

Goliasch, J., & Nelson, L. 2015, ApJ, 809, 80

Green, R. F., Ferguson, D. H., Liebert, J., & Schmidt, M. 1982, PASP, 94, 560

Haakonsen, C. B., & Rutledge, R. E. 2009, ApJS, 184, 138

Halpern, J. P., & Thorstensen, J. R. 2015, AJ, 150, 170

Haswell, C. A., Horne, K., Thomas, G., Patterson, J., & Thorstensen, J. R. 1994, Interacting Binary Stars, 56, 268

Henden, A. A., Levine, S., Terrell, D., & Welch, D. L. 2015, American Astronomical Society Meeting Abstracts, 225, #336.16

Kato, T., Maehara, H., Uemura, M., et al. 2010, PASJ, 62, 1525

Kato, T., Hambsch, F.-J., Maehara, H., et al. 2013, PASJ, 65, 23

Kato, T., Hambsch, F.-J., Maehara, H., et al. 2014, PASJ, 66, 30

Kato, T., Hambsch, F.-J., Dubovsky, P. A., et al. 2015, PASJ, 67, 105

Kaur, A., Porter, A., Wilber, A., et al. 2014, The Astronomer's Telegram, 6624, 1

Kepler, S. O., Pelisoli, I., Koester, D., et al. 2016, MNRAS, 455, 3413

Knigge, C. 2006, MNRAS, 373, 484

Kurtz, M. J. & Mink, D. J. 1998, PASP, 110, 934

Lazavera, A., Voroshilov, N., Denisenko, D., Kuznetsov, A., Gorbovskoy, E., & Lipunov, V. 2013, arXiv:1307:6855

Lipunov, V., Kornilov, V., Gorbovskoy, E., et al. 2010, Advances in Astronomy, 2010, 349171

McLaughlin, D. B. 1924, ApJ, 60, 22

Monet, D. G., Levine, S. E., Canzian, B., et al. 2003, AJ, 125, 984

Patterson, J. 1998, PASP, 110, 1132

Rebassa-Mansergas, A., Parsons, S. G., Copperwheat, C. M., et al. 2014, ApJ, 790, 28

Ringwald, F. A. 1993, PASP, 105, 805

Ritter, H., & Kolb, U. 2003, A&A, 404, 301

Roeser, S., Demleitner, M., & Schilbach, E. 2010, AJ, 139, 2440

Rossiter, R. A. 1924, ApJ, 60,

Schlegel, D. J., Finkbeiner, D. P., & Davis, M. 1998, ApJ, 500, 525 2440

Schneider, D. and Young, P. 1980, ApJ, 238, 946

Schwope, A. D., & Thinius, B. 2012, Astronomische Nachrichten, 333, 717

Shappee, B., Kochanek, C. S., Stanek, K. Z., et al. 2013a, The Astronomer's Telegram, 4987, 1

Shappee, B. J., Prieto, J. L., Grupe, D., et al. 2014b, ApJ, 788, 48

Szkody, P., Anderson, S. F., Brooks, K., et al. 2011, AJ, 142, 181

Szkody, P., Everett, M. E., Howell, S. B., et al. 2014, AJ, 148, 63

Thorstensen, J. R. 2003, AJ, 126, 3017

Thorstensen, J. R., & Freed, I. W. 1985, AJ, 90, 2082

Thorstensen, J. R., Ringwald, F. A., Wade, R. A., Schmidt, G. D., & Norsworthy, J. E. 1991, AJ, 102, 272

Thorstensen, J. R. 2015, PASP, 127, 351

Thorstensen, J. R., & Armstrong, E. 2005, AJ, 130, 759

Thorstensen, J. R., & Skinner, J. N. 2012, AJ, 144, 81

Thorstensen, J. R., & Halpern, J. 2013, AJ, 146, 107

Thorstensen, J. R. 2013, PASP, 125, 506

Thorstensen, J. R. 2015, PASP, 127, 351

Tiurina, N., Frolova, N., Pruzghinskaya, M., et al. 2013, The Astronomer's Telegram, 4871, 1

Tonry, J., & Davis, M. 1979, AJ, 84, 1511

Warner, B. 1987, MNRAS, 227, 23

Warner, B., in *Cataclysmic Variable Stars*, 1995, Cambridge University Press, New York

West, A. A., Hawley, S. L., Bochanski, J. J., et al. 2008, AJ, 135, 785

Zacharias, N., Finch, C., Subasavage, J., et al. 2015, VizieR Online Data Catalog, 1329, 0

Zharikov, S., Tovmassian, G., Aviles, A., et al. 2013, A&A, 549, A77

This preprint was prepared with the AAS LaTeX macros v5.2.

Table 1. List of Objects

Short Name	Other Name	α_{2000} [h m s]	δ_{2000} [° ′ ″]	Type
CSS0015+26	CSS090918:001538+263657	0 15 38.26	+26 36 56.8	UG(SU)
ASAS-SN 14dr		0 36 40.27	+23 08 33.2	UG(SU)
CSS0133+38	CSS091027:013309+383217	1 33 08.72	+38 32 17.2	UG(SU)
CSS0143+26	CSS141029:014305+263833	1 43 04.69	+26 38 33.0	UG(SU)
OT0150+37	MASTER J015017.0+375614	1 50 16.19	+37 56 19.0	UG:
CSS0208+37	CSS101207:020804+373217	2 08 04.23	+37 32 16.6	UG(SU)
ASAS-SN 14dx		2 34 27.59	−04 54 34.3	UGSU; PM
CSS0357+10	CSS091109:035759+102943	3 57 58.67	+10 29 42.9	Polar
CSS0500+13	CSS151201:050027+133420	5 00 27.24	+13 34 20.0	UG; 2ndary
OT0647+49	MASTER J064725.70+491543.9	6 47 25.70	+49 15 43.9	UGSU
ASAS-SN 14kj		8 02 34.39	−00 09 40.2	UG: (SU)
ASAS-SN 15cw		8 08 18.98	+00 59 00.1	UG:; ecl
ASAS-SN 14ag		8 13 18.52	−01 03 29.5	UGSU; ecl; PM
ASAS-SN 14ak		9 50 57.04	−29 46 46.0	UG(SU)
CSS1028−16	CSS140309:102844-161303	10 28 43.87	−16 13 03.4	UG:(ZC?)
SDSS1029+48	SDSS J102905.21+485515.23	10 29 05.24	+48 55 15.2	UG:(WZ?)
ASAS-SN 15aa		10 49 25.91	−21 47 35.9	UG; ecl; 2ndary
CSS1055+09	CSS080130:105550+095621	10 55 50.08	+09 56 20.5	UG; 2ndary
CSS1211−08	CSS110205:121119-083957	12 11 19.13	−08 39 57.1	UG(SU)
SDSS1429+00	SDSS J142958.15+000319.6	14 29 58.15	+00 03 19.6	NL
ASAS-SN 15dl		16 22 00.39	−22 41 17.0	UG
CSS1631+10	CSS080505:163121+103134	16 31 20.89	+10 31 33.9	UG
CSS1702+55	CSS130416:170209+551827	17 02 08.59	+55 18 26.7	UG(SU)
OT1727+38	MASTER J172758.09+380021.5	17 27 58.14	+38 00 22.5	UG(SU)
ASAS-SN 15cm		17 31 02.21	+34 26 33.1	UG; 2ndary
CSS1735+15	CSS110623:173517+154708	17 35 16.91	+15 47 08.4	UG; 2ndary
OT1759+14	MASTER J175908.60+145130.2	17 59 08.60	+14 51 30.2	UG; 2ndary
DDE23		18 19 33.12	+58 06 26.3	Polar
ASAS-SN 13bs		18 30 08.84	+37 36 41.6	UG: (SU)
DDE14	1RXS J185310.0+594509	18 53 09.61	+59 45 06.8	UGSU
CSS2133+19	CSSJ213319.4+190155	21 33 19.47	+19 01 55.0	UG; 2ndary
CSS2156+19	CSS090622:215636+193242	21 56 36.32	+19 32 41.9	UG(SU); ecl
CSS2227+28	CSS090531:222724+284404	22 27 24.49	+28 44 03.8	UG(SU)
CSS2319+33	CSS111021:231909+331540	23 19 09.18	+33 15 39.8	NL
CSS2335+12	CSS131214:233546+123448	23 35 45.95	+12 34 48.4	Polar

Note. — Coordinates are for the most part from SDSS or the PPMXL catalog (Roeser et al. 2010). In the last column, the notation is as follows: UG – U Gem star, or dwarf nova, with a colon indicating that this is uncertain because outbursts have not been reported; UG(SU) – U Gem star in the period

range in which superhumps may be expected, but for which they have not been reported; UGSU – SU UMa star with measured superhump period; UG:(WZ?) – apparently slow mass transfer dwarf nova without reported outbursts; UG:(ZC?) – possible Z Cam-type dwarf nova; Polar – AM Her star; PM – significant proper motion; 2ndary – secondary star detected in spectrum; ecl – eclipses are detected.

Table 2. Radial Velocities

Star SDSS J	Time[a]	$v_{\rm emn}$ [km s^{-1}]	σ [km s^{-1}]	$v_{\rm abs}$ [km s^{-1}]	σ [km s^{-1}]
CSS0015+26	2456942.9461	12	8	···	···
CSS0015+26	2456942.9535	11	9	···	···
CSS0015+26	2456942.9608	52	10	···	···
CSS0015+26	2456943.6660	47	8	···	···
CSS0015+26	2456943.6733	28	9	···	···
CSS0015+26	2456943.6807	14	9	···	···
CSS0015+26	2456943.6880	-2	10	···	···
CSS0015+26	2456943.6953	-8	10	···	···

[a]Barycentric Julian Date of mid-exposure. The time base is UTC.

Note. — Table 2 is published in its entirety in the electronic edition of The Astronomical Journal, A portion is shown here for guidance regarding its form and content.

Table 3. Fits to Radial Velocities

Data set	T_0[a]	P (d)	K (km s^{-1})	γ (km s^{-1})	N	σ[b] (km s^{-1})
CSS0015+26	56944.8652(11)	0.10150(6)	77(4)	−36(3)	28	11
ASAS-SN 14dr	57317.9693(15)	0.06655(9)	59(8)	−67(6)	49	27
CSS0133+38	56944.968(3)	0.07497(13)	47(10)	−4(8)	41	26
CSS0143+26	57002.655(2)	0.0646(2)	47(9)	−33(6)	36	21
OT0150+37	56597.871(3)	0.1481(3)	84(10)	−31(7)	58	32
CSS0208+37	56300.6700(16)	0.05845(9)	63(11)	−55(8)	58	36
ASAS-SN 14dx	56945.8452(7)	0.05756(6)	41(3)	8(2)	43	10
CSS0357+10	56298.6443(7)	0.07918(6)	320(19)	11(13)	33	62
CSS0500+13	57440.7942(9)	0.15465(3)	126(5)	−6(3)	46	16
OT0647+49	57000.9276(14)	0.06554(12)[c]	78(10)	−30(7)	55	33
ASAS-SN 14kj	57433.935(3)	0.0906(2)	82(18)	14(13)	45	42
ASAS-SN 15cw	57430.9527(18)	0.0791258(4)[d]	78(12)	−40(8)	13	22
ASAS-SN 14ag	57402.8461(17)	0.060310651(2)[d]	100(19)	31(13)	44	43
ASAS-SN 14ak	57433.7837(14)	0.08869(7)	73(7)	4(5)	33	17
CSS1028−16	57460.869(4)	0.1897(6)	102(12)	−3(9)	53	40
SDSS1029+48	57430.7432(18)	0.063421(8)	22(4)	−10(3)	58	13
ASAS-SN 15aa [abs.]	57109.974(3)	0.375540(2)[e]	175(7)	−23(5)	38	23
ASAS-SN 15aa [emn.]	57109.788(7)	···	154(14)	−66(11)	34	55
CSS1055+09	57436.0463(16)	0.1624(5)	116(6)	−75(5)	36	16
CSS1211−08	57438.840(2)	0.07913(19)	45(8)	−26(6)	47	22
SDSS1429+00	57460.7595(16)	0.14833(17)	172(14)	−28(9)	53	42
ASAS-SN 15dl	57142.780(5)	0.2288(9)	82(12)	−5(8)	49	28
(alternate)	57142.741(8)	0.2976(18)	80(14)	−6(10)	49	31
CSS1631+10	55323.9928(19)	0.06265(11)[c]	60(12)	−35(8)	115	38
CSS1702+55	56453.6424(16)	0.06931(15)	35(5)	−27(4)	33	12
OT1727+38	57554.7680(15)	0.05704(4)	53(8)	−25(6)	56	27
ASAS-SN 15cm	57553.8461(11)	0.208466(2)[f]	229(7)	21(5)	21	18
CSS1735+15 [abs.]	56827.9769(15)	0.3534(10)[g]	136(4)	−35(3)	27	10

Table 3—Continued

Data set	T_0[a]	P (d)	K (km s^{-1})	γ (km s^{-1})	N	σ[b] (km s^{-1})
CSS1735+15 [emn.]	56827.826(6)	···	101(15)	−66(9)	27	29
OT1759+14 [abs.]	56830.778(4)	0.2987(8)[h]	196(14)	45(11)	17	23
OT1759+14 [emn.]	56830.930(12)	···	72(15)	39(12)	17	24
DDE23	56453.8746(9)	0.09207(9)	318(21)	36(14)	19	41
ASAS-SN 13bs	56551.7588(16)	0.05725(8)[c]	45(8)	−68(6)	53	18
DDE14	56831.9706(16)	0.05826(9)	73(15)	−22(10)	33	33
CSS2133+19 [abs.]	56942.727(4)	0.3761(5)[h]	151(8)	52(7)	18	19
CSS2133+19 [emn.]	56942.925(4)	···	120(7)	10(5)	20	15
CSS2227+28	56944.6401(16)	0.09101(18)	48(5)	−27(4)	27	12
CSS2319+33	56551.6415(17)	0.14616(19)	96(8)	10(5)	31	18
CSS2335+12	57001.7433(19)	0.1618(7)	169(13)	−25(9)	37	31

Note. — Parameters of least-squares sinusoid fits to the radial velocities, of the form $v(t) = \gamma + K \sin(2\pi(t - T_0)/P$.

[a]Heliocentric Julian Date minus 2400000. The epoch is chosen to be near the center of the time interval covered by the data, and within one cycle of an actual observation.

[b]RMS residual of the fit.

[c]Period given is the weighted mean of periods from separate fits to the velocities from the individual observing runs.

[d]Period fixed at value derived from eclipses.

[e]For both the absorption and emission fits, the period was held fixed at the value derived from the ellipsoidal variations in the archival CRTS light curve.

[f]Period fixed at the value derived from the archival CRTS light curve.

[g]Period for emission held fixed at the value derived from the absorption lines.

[h]Period was fixed at the weighted mean of the absorption- and emission-line periods.

Table 4. Eclipse Timings

E	T	$O-C$	Instrument
ASAS-SN 15cw :			
$2457431.7674(1) + 0.0791258(4)E$			
−1	7431.6881	−17	1.3m+Andor
0	7431.7675	+8	1.3m+Andor
11	7432.6377	−12	1.3m+Andor
12	7432.7171	10	1.3m+Andor
27	7433.9039	7	1.3m+Andor
112	7440.6295	7	1.3m+Andor
391	7462.7056	−2	1.3m+slit
ASAS-SN 14ag:			
$2457416.7385(1) + 0.060310651(2)E$			
0	7416.7386	9	1.3m+Andor
1	7416.7987	−10	1.3m+Andor
2	7416.8591	−2	1.3m+Andor
34	7418.7892	12	1.3m+Andor
35	7418.8495	11	1.3m+Andor
ASAS-SN 15aa:			
$2457109.977(3) + 0.375540(2)E$			
−6	7107.7234	−31	1.3m+slit
2	7110.7286	45	1.3m+slit
34	7122.7460	55	1.3m+Andor
783	7404.0242	−54	1.3m+Andor
788	7405.9014	−97	1.3m+Andor
CSS2156+19:			
$2456941.7307(4) + 0.0709291(1)E$			
0	6941.73075	4	1.3m+Andor
27	6943.64588	8	1.3m+Andor
28	6943.717	25	1.3m+Andor
29	6943.7878	13	1.3m+Andor
41	6944.63839	−35	1.3m+Andor
42	6944.70959	−11	1.3m+Andor
6075[a]	7372.6244	0	1.3m+Andor

Note. — Column 1: Integer cycle count E in the quoted ephemeris. Column 2: the observed time of mid-eclipse, given as the barycentric

Julian Date minus 2,450,000. Column 3: Observed timing, minus the time predicted by the quoted ephemeris, in seconds. Column 4: Telescope and instrument; *slit* means that the Andor camera was viewing the spectrograph slit jaws.

[a]This observation was kindly obtained by Karolina Bakowska.

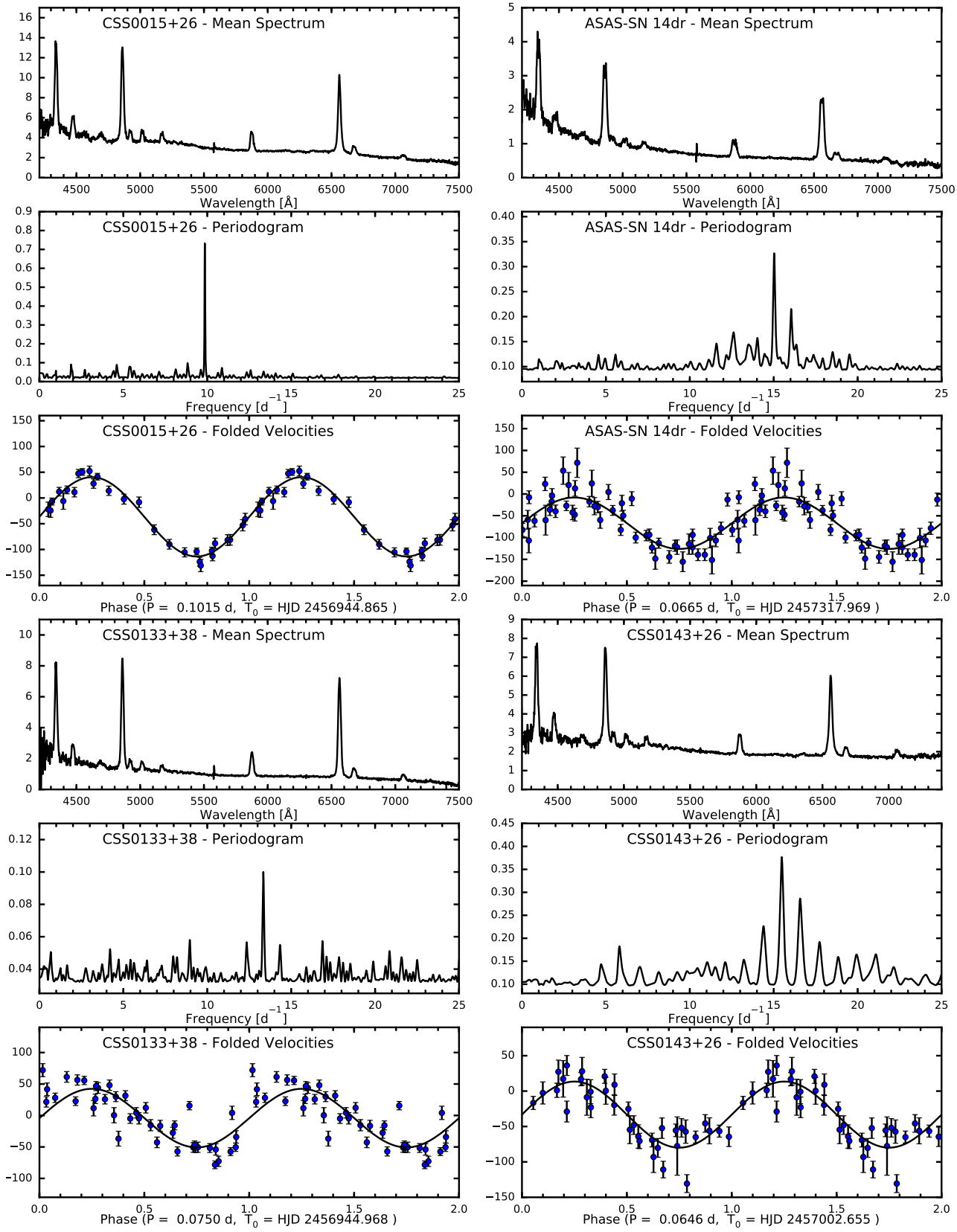
CSS0015+26 - Mean Spectrum
Wavelength [Å]
ASAS-SN 14dr - Mean Spectrum
Wavelength [Å]
CSS0015+26 - Periodogram
Frequency [d^{-1}]
ASAS-SN 14dr - Periodogram
Frequency [d^{-1}]
CSS0015+26 - Folded Velocities
Phase (P = 0.1015 d, T$_0$ = HJD 2456944.865)
ASAS-SN 14dr - Folded Velocities
Phase (P = 0.0665 d, T$_0$ = HJD 2457317.969)
CSS0133+38 - Mean Spectrum
Wavelength [Å]
CSS0143+26 - Mean Spectrum
Wavelength [Å]
CSS0133+38 - Periodogram
Frequency [d^{-1}]
CSS0143+26 - Periodogram
Frequency [d^{-1}]
CSS0133+38 - Folded Velocities
Phase (P = 0.0750 d, T$_0$ = HJD 2456944.968)
CSS0143+26 - Folded Velocities
Phase (P = 0.0646 d, T$_0$ = HJD 2457002.655)

Fig. 1.— Average spectra, periodograms, and folded velocity curves for CSS0015+26, ASAS-SN 14dr, CSS0133+38, and CSS0143+26. The vertical scales, unlabeled to save space, are (1) for the spectra, f_λ in units of 10^{-16} erg s^{-1} cm^{-2} Å^{-1}; (2) for the periodograms, $1/\chi^2$ (dimensionless); and (3) for the radial velocity curves, barycentric radial velocity in km s^{-1}. When two traces are shown in the spectral plot, the lower trace shows the average spectrum minus a late-type spectrum scaled to match the spectrum of the secondary star. In cases where velocities are from more than one observing run, the periodogram is labeled with the word "peaks", because the curve shown formed by joining local maxima in the full periodogram with straight lines. This suppresses fine-scale ringing due to the unknown number of cycle counts between runs. The folded velocity curves all show the same data plotted over two cycles for continuity, and the best-fit sinusoid (see Table 3) is also plotted. The velocities shown are normally Hα emission velocities. Secondary-star cross-correlation velocities, when available, are shown in red, together with the best-fit sinusoid. The error bars for the emission lines are computed by propagating the estimated noise in the spectrum through the measurment, and hence do not include jitter due to line profile variations.

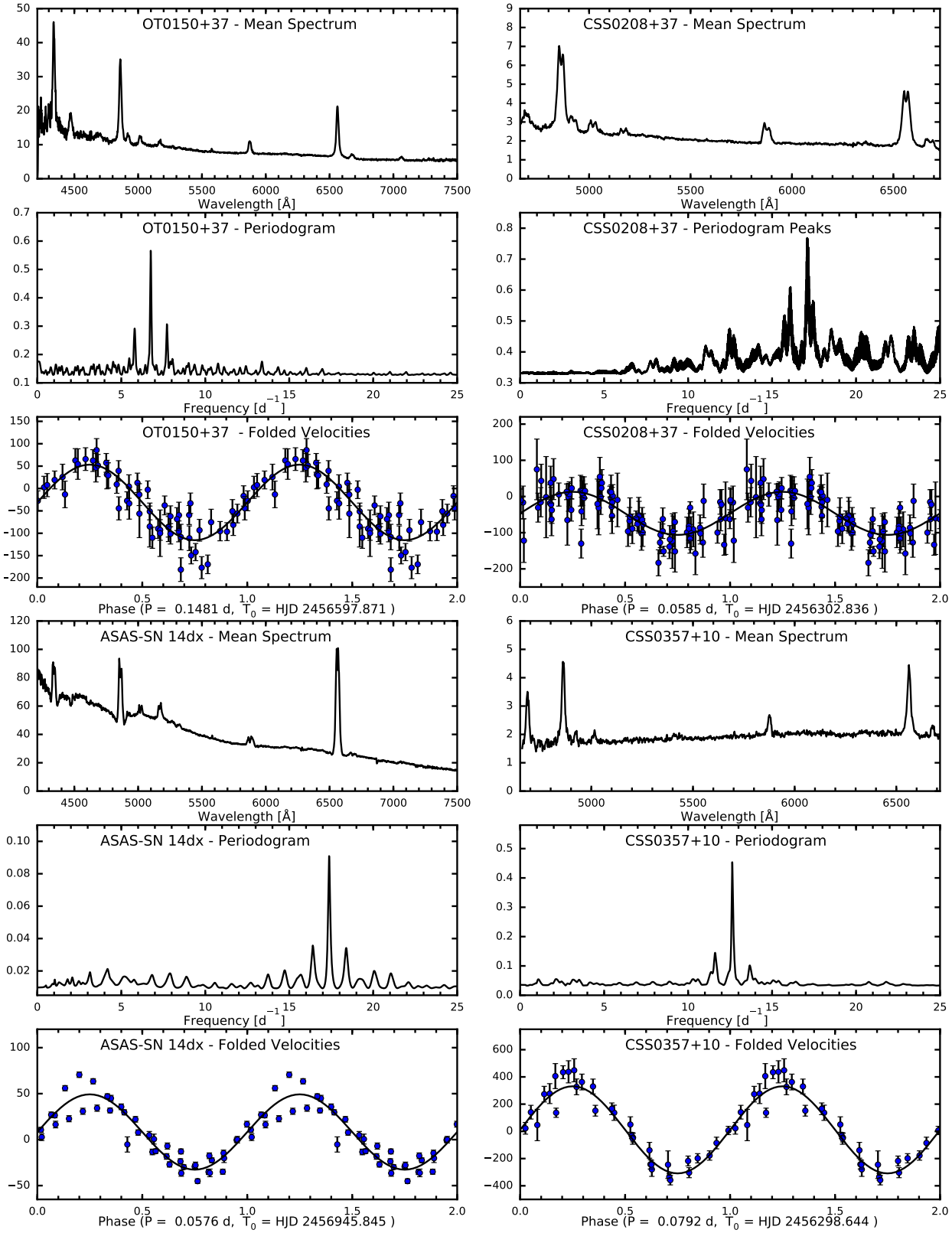
OT0150+37 - Mean Spectrum
Wavelength [Å]
CSS0208+37 - Mean Spectrum
Wavelength [Å]
OT0150+37 - Periodogram
Frequency [d^{-1}]
CSS0208+37 - Periodogram Peaks
Frequency [d^{-1}]
OT0150+37 - Folded Velocities
Phase (P = 0.1481 d, T$_0$ = HJD 2456597.871)
CSS0208+37 - Folded Velocities
Phase (P = 0.0585 d, T$_0$ = HJD 2456302.836)
ASAS-SN 14dx - Mean Spectrum
Wavelength [Å]
CSS0357+10 - Mean Spectrum
Wavelength [Å]
ASAS-SN 14dx - Periodogram
Frequency [d^{-1}]
CSS0357+10 - Periodogram
Frequency [d^{-1}]
ASAS-SN 14dx - Folded Velocities
Phase (P = 0.0576 d, T$_0$ = HJD 2456945.845)
CSS0357+10 - Folded Velocities
Phase (P = 0.0792 d, T$_0$ = HJD 2456298.644)

Fig. 2.— Similar to Fig. 1, but for OT O150+37, CSS 0208+37, ASAS-SN 14dx, and CSS 0357+10.

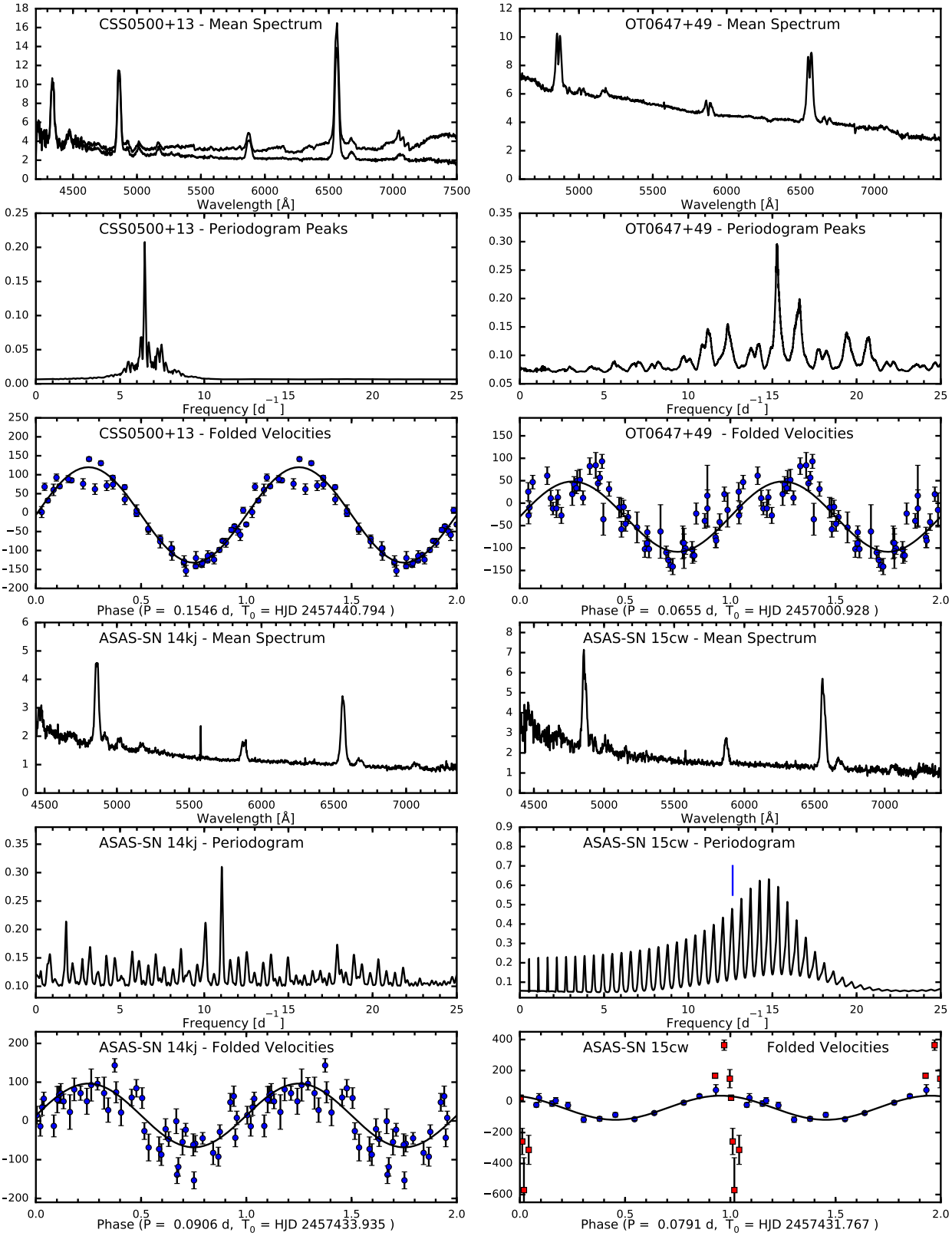
CSS0500+13 - Mean Spectrum
Wavelength [Å]
OT0647+49 - Mean Spectrum
Wavelength [Å]
CSS0500+13 - Periodogram Peaks
Frequency [d^{-1}]
OT0647+49 - Periodogram Peaks
Frequency [d^{-1}]
CSS0500+13 - Folded Velocities
Phase (P = 0.1546 d, T$_0$ = HJD 2457440.794)
OT0647+49 - Folded Velocities
Phase (P = 0.0655 d, T$_0$ = HJD 2457000.928)
ASAS-SN 14kj - Mean Spectrum
Wavelength [Å]
ASAS-SN 15cw - Mean Spectrum
Wavelength [Å]
ASAS-SN 14kj - Periodogram
Frequency [d^{-1}]
ASAS-SN 15cw - Periodogram
Frequency [d^{-1}]
ASAS-SN 14kj - Folded Velocities
Phase (P = 0.0906 d, T$_0$ = HJD 2457433.935)
ASAS-SN 15cw Folded Velocities
Phase (P = 0.0791 d, T$_0$ = HJD 2457431.767)

Fig. 3.— (Caption on next page.)

Fig. 3.— Similar to Fig. 1, but for CSS0500+13, OT 0647+49, ASAS-SN 14kj, and ASAS-SN 15cw. For CSS0500+13, the upper trace shows the mean spectrum, and the lower trace shows the result of subtracting a scaled spectrum of Gliese 388, an M3.5 dwarf. For the folded velocities on ASAS-SN 15cw, the zero of phase is chosen to correspond to the eclipse. The red points show the pronounced rotational disturbance near eclipse and were not included in the sinusoid fit. The period for this star was inferred from eclipses, rather than the velocity periodogram; the vertical line in the periodogram plot indicates the period.

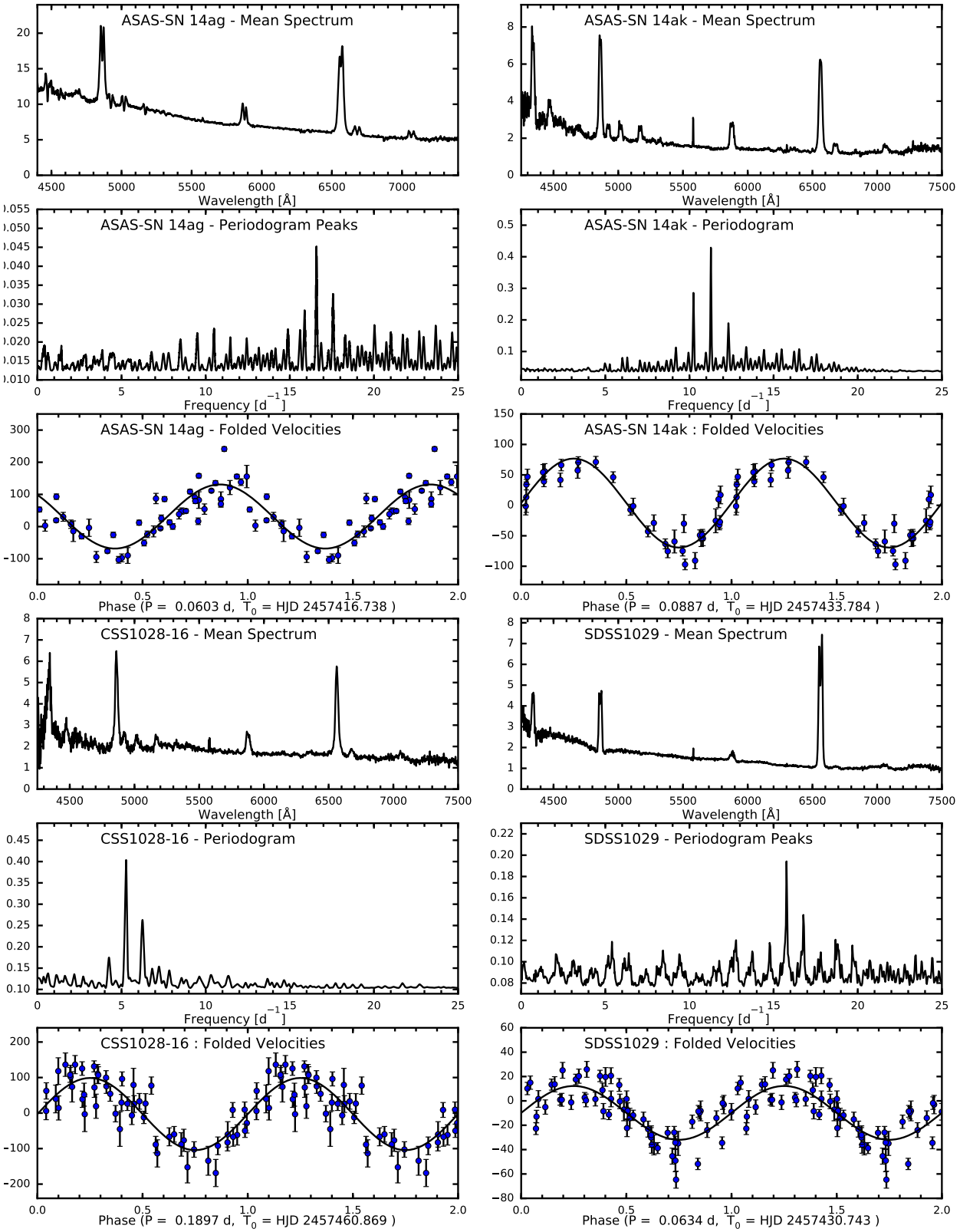
ASAS-SN 14ag - Mean Spectrum
Wavelength [Å]
ASAS-SN 14ak - Mean Spectrum
Wavelength [Å]
ASAS-SN 14ag - Periodogram Peaks
Frequency [d^{-1}]
ASAS-SN 14ak - Periodogram
Frequency [d^{-1}]
ASAS-SN 14ag - Folded Velocities
Phase (P = 0.0603 d, T$_0$ = HJD 2457416.738)
ASAS-SN 14ak : Folded Velocities
Phase (P = 0.0887 d, T$_0$ = HJD 2457433.784)
CSS1028-16 - Mean Spectrum
Wavelength [Å]
SDSS1029 - Mean Spectrum
Wavelength [Å]
CSS1028-16 - Periodogram
Frequency [d^{-1}]
SDSS1029 - Periodogram Peaks
Frequency [d^{-1}]
CSS1028-16 : Folded Velocities
Phase (P = 0.1897 d, T$_0$ = HJD 2457460.869)
SDSS1029 : Folded Velocities
Phase (P = 0.0634 d, T$_0$ = HJD 2457430.743)

Fig. 4.— Similar to Fig. 1, but for ASAS-SN 14ag, ASAS-SN 14ak, CSS 1028−16, and SDSS 1029.

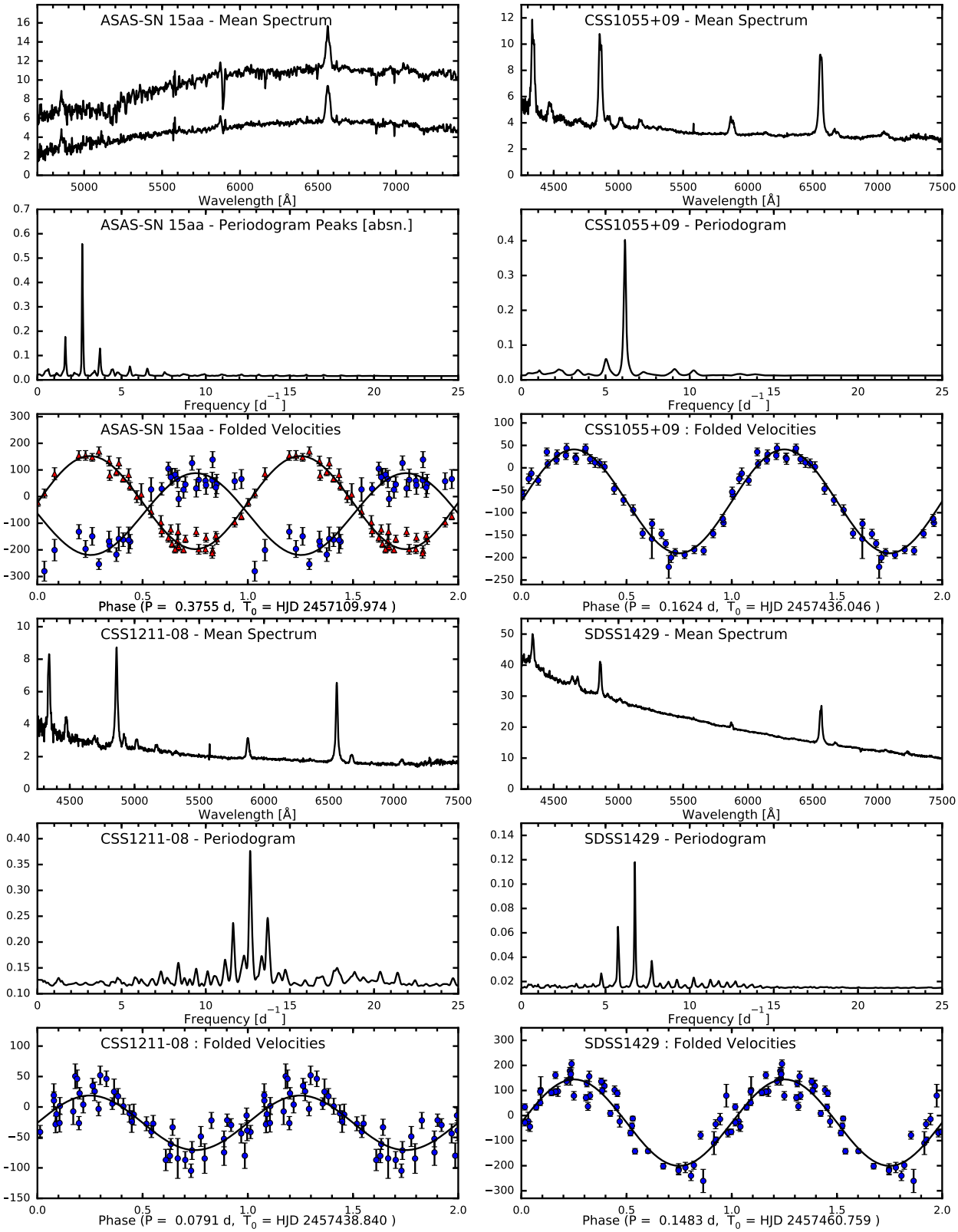
ASAS-SN 15aa - Mean Spectrum
Wavelength [Å]
CSS1055+09 - Mean Spectrum
Wavelength [Å]
ASAS-SN 15aa - Periodogram Peaks [absn.]
Frequency [d^{-1}]
CSS1055+09 - Periodogram
Frequency [d^{-1}]
ASAS-SN 15aa - Folded Velocities
Phase (P = 0.3755 d, T$_0$ = HJD 2457109.974)
CSS1055+09 : Folded Velocities
Phase (P = 0.1624 d, T$_0$ = HJD 2457436.046)
CSS1211-08 - Mean Spectrum
Wavelength [Å]
SDSS1429 - Mean Spectrum
Wavelength [Å]
CSS1211-08 - Periodogram
Frequency [d^{-1}]
SDSS1429 - Periodogram
Frequency [d^{-1}]
CSS1211-08 : Folded Velocities
Phase (P = 0.0791 d, T$_0$ = HJD 2457438.840)
SDSS1429 : Folded Velocities
Phase (P = 0.1483 d, T$_0$ = HJD 2457460.759)

Fig. 5.— Similar to Fig. 1, but for ASAS-SN 15aa, CSS1055+09, CSS1211−08, and SDSS1429.

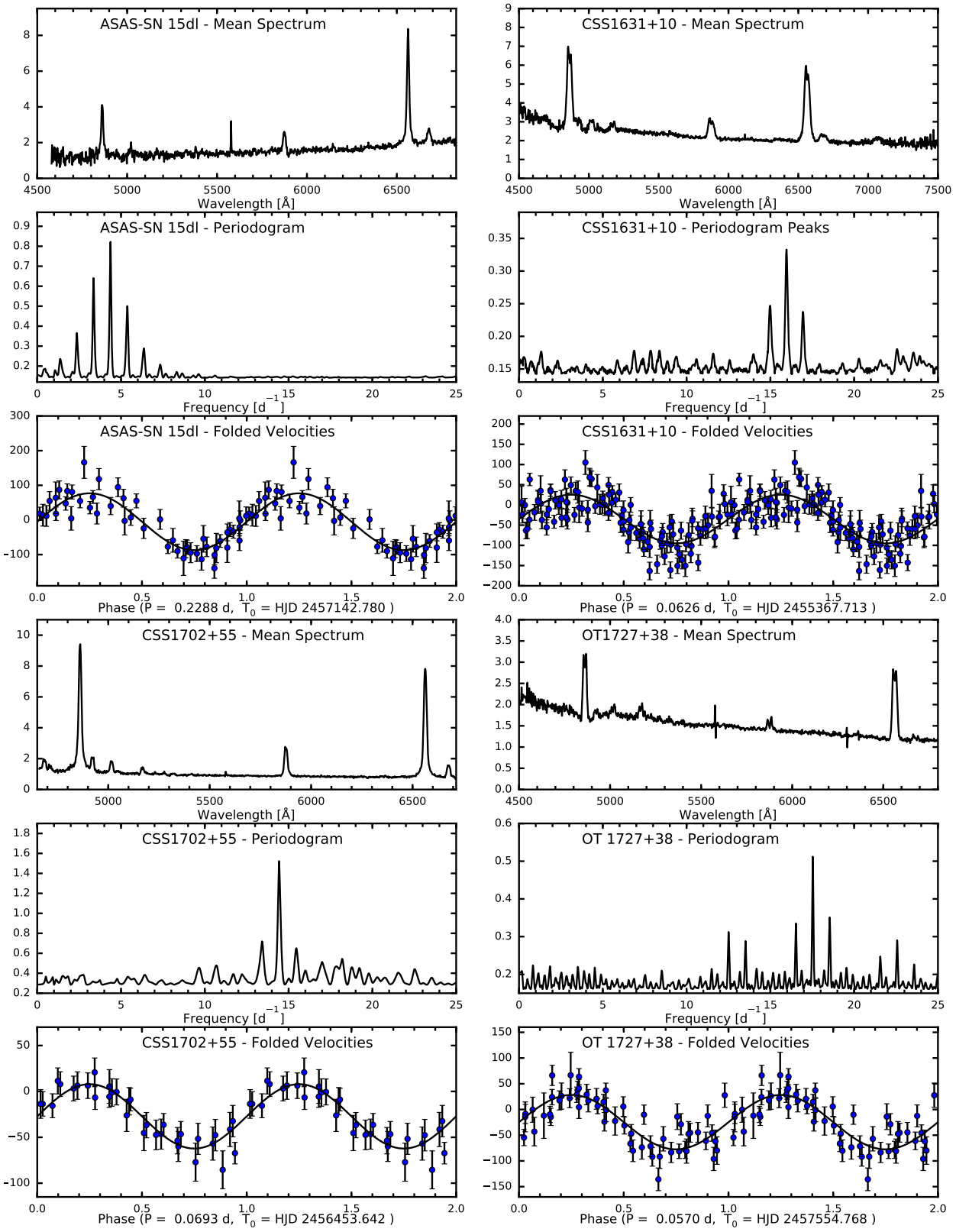
ASAS-SN 15dl - Mean Spectrum
Wavelength [Å]
CSS1631+10 - Mean Spectrum
Wavelength [Å]
ASAS-SN 15dl - Periodogram
Frequency [d^{-1}]
CSS1631+10 - Periodogram Peaks
Frequency [d^{-1}]
ASAS-SN 15dl - Folded Velocities
Phase (P = 0.2288 d, T$_0$ = HJD 2457142.780)
CSS1631+10 - Folded Velocities
Phase (P = 0.0626 d, T$_0$ = HJD 2455367.713)
CSS1702+55 - Mean Spectrum
Wavelength [Å]
OT1727+38 - Mean Spectrum
Wavelength [Å]
CSS1702+55 - Periodogram
Frequency [d^{-1}]
OT 1727+38 - Periodogram
Frequency [d^{-1}]
CSS1702+55 - Folded Velocities
Phase (P = 0.0693 d, T$_0$ = HJD 2456453.642)
OT 1727+38 - Folded Velocities
Phase (P = 0.0570 d, T$_0$ = HJD 2457554.768)

Fig. 6.— Similar to Fig. 1, but for ASAS-SN 15dl, CSS1631+10, CSS1702+55, and OT1727+38.

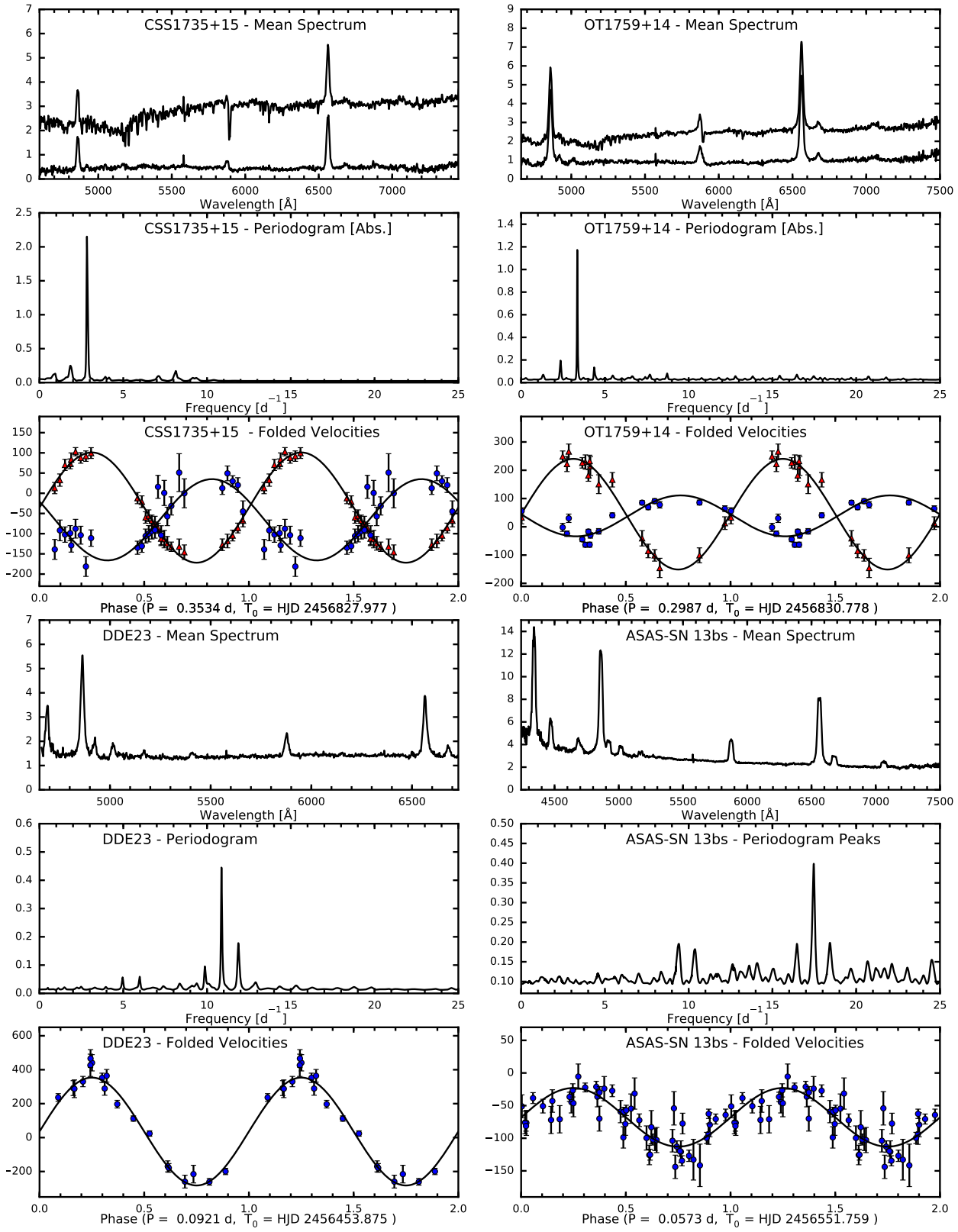
CSS1735+15 - Mean Spectrum
Wavelength [Å]
OT1759+14 - Mean Spectrum
Wavelength [Å]
CSS1735+15 - Periodogram [Abs.]
Frequency [d^{-1}]
OT1759+14 - Periodogram [Abs.]
Frequency [d^{-1}]
CSS1735+15 - Folded Velocities
Phase (P = 0.3534 d, T$_0$ = HJD 2456827.977)
OT1759+14 - Folded Velocities
Phase (P = 0.2987 d, T$_0$ = HJD 2456830.778)
DDE23 - Mean Spectrum
Wavelength [Å]
ASAS-SN 13bs - Mean Spectrum
Wavelength [Å]
DDE23 - Periodogram
Frequency [d^{-1}]
ASAS-SN 13bs - Periodogram Peaks
Frequency [d^{-1}]
DDE23 - Folded Velocities
Phase (P = 0.0921 d, T$_0$ = HJD 2456453.875)
ASAS-SN 13bs - Folded Velocities
Phase (P = 0.0573 d, T$_0$ = HJD 2456551.759)

Fig. 7.— Similar to Fig. 1, but for CSS1735+15, OT1759+14, DDE23, and ASAS-SN 13bs.

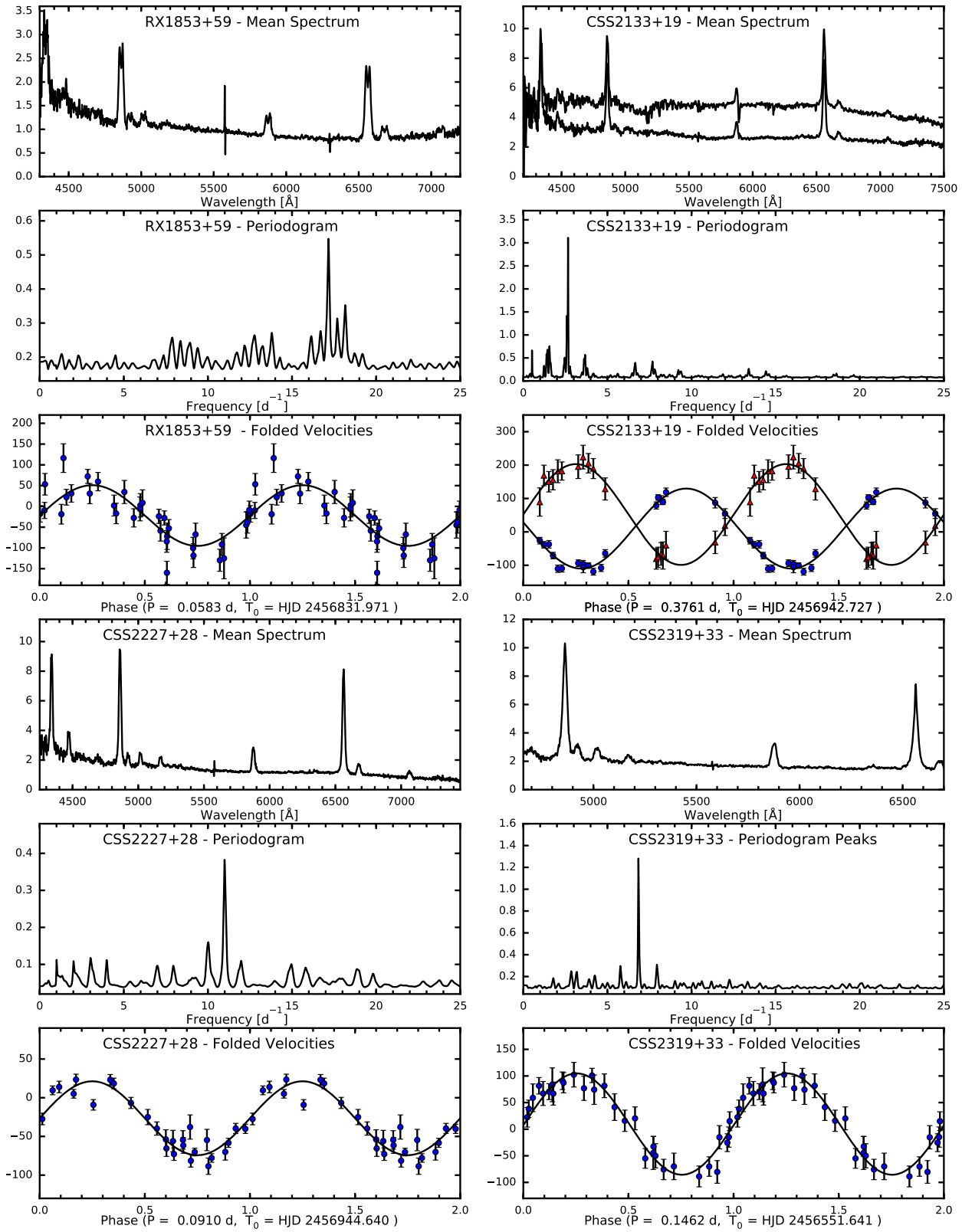
RX1853+59 - Mean Spectrum
Wavelength [Å]
CSS2133+19 - Mean Spectrum
Wavelength [Å]
RX1853+59 - Periodogram
Frequency [d^{-1}]
CSS2133+19 - Periodogram
Frequency [d^{-1}]
RX1853+59 - Folded Velocities
Phase (P = 0.0583 d, T$_0$ = HJD 2456831.971)
CSS2133+19 - Folded Velocities
Phase (P = 0.3761 d, T$_0$ = HJD 2456942.727)
CSS2227+28 - Mean Spectrum
Wavelength [Å]
CSS2319+33 - Mean Spectrum
Wavelength [Å]
CSS2227+28 - Periodogram
Frequency [d^{-1}]
CSS2319+33 - Periodogram Peaks
Frequency [d^{-1}]
CSS2227+28 - Folded Velocities
Phase (P = 0.0910 d, T$_0$ = HJD 2456944.640)
CSS2319+33 - Folded Velocities
Phase (P = 0.1462 d, T$_0$ = HJD 2456551.641)

Fig. 8.— Similar to Fig. 1, but for RX1853+59, CSS2133+19, CSS2227+28, and CSS2319+33.

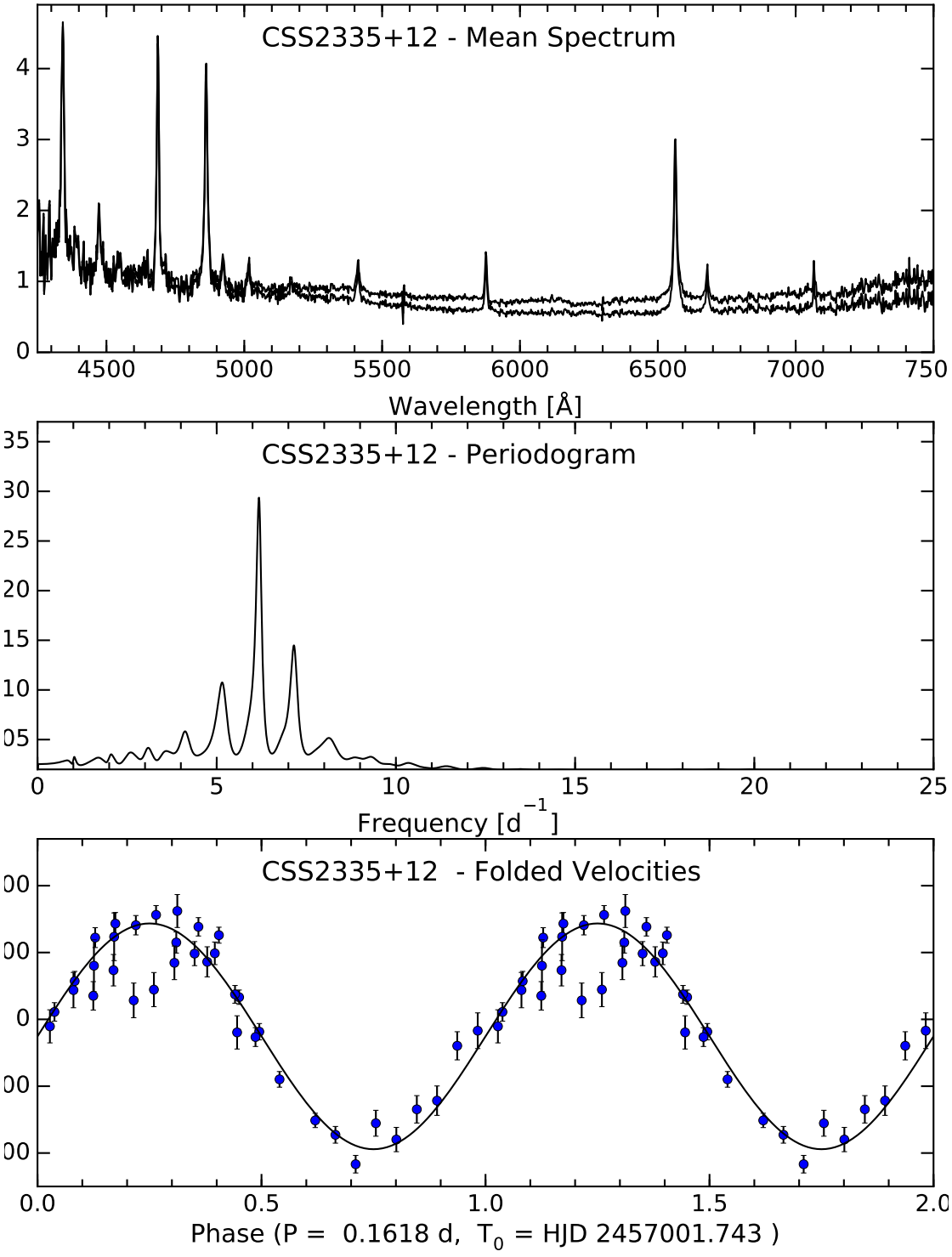
CSS2335+12 - Mean Spectrum
Wavelength [Å]
CSS2335+12 - Periodogram
Frequency [d^{-1}]
CSS2335+12 - Folded Velocities
Phase (P = 0.1618 d, T$_0$ = HJD 2457001.743)

Fig. 9.— Similar to Fig. 1, but for CSS2335+12.

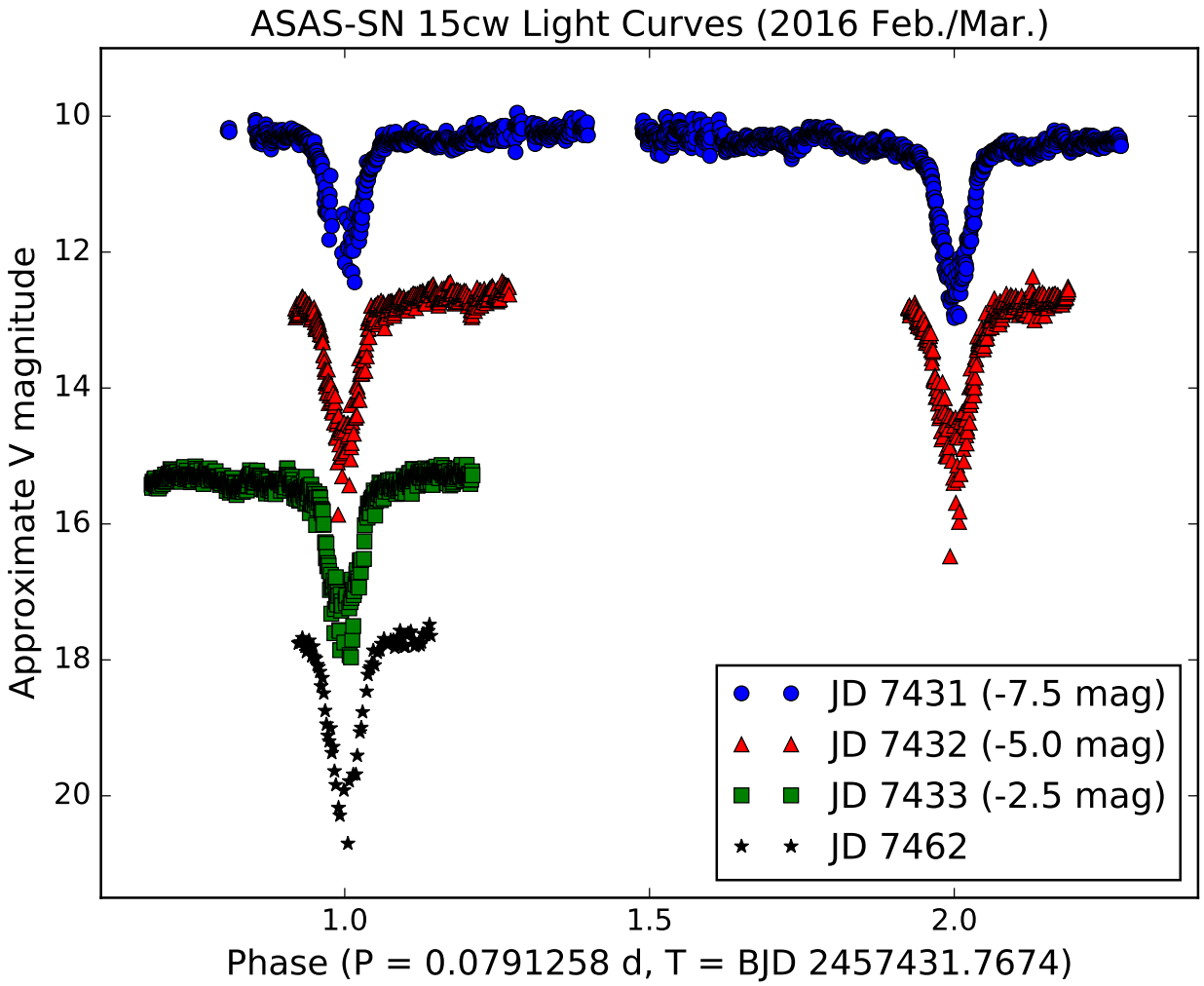

Fig. 10.— Light curves of ASAS-SN 15cw taken in 2016 February and March. The horizontal axis shows the phase on the indicated ephemeris, and each night is offset by 2.5 mag The vertical axis shows the differential magnitude in white light, adjusted to rough V magnitude by adding the magnitude of the comparison star at α =08:08:21.37, δ =00:59:15.7, 39″ from the program object in position angle 67 degrees, for which APASS (Henden et al. 2015) gives $V = 15.67$.

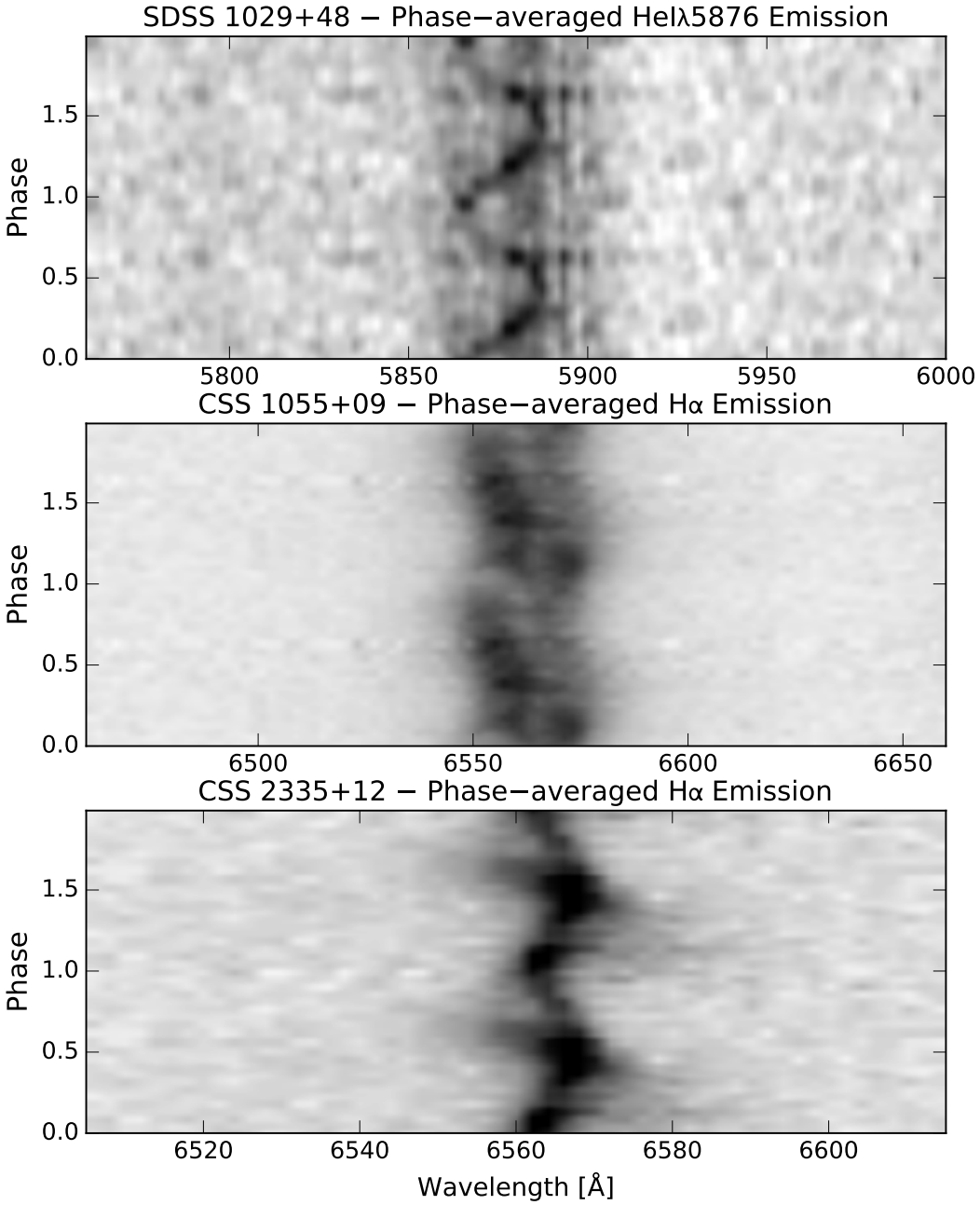

Fig. 11.— (Top panel). Phase averaged greyscale representation of the HeI λ5876 emission line in CSS 1029+48. The color map is inverted (emission appears dark). Each line of the image is a weighted average of spectra taken near the appropriate phase. Before averaging, the individual spectra were rectified (i.e., divided by a fitted continuum), and bad pixels were edited out. The data are repeated for a second cycle. A clear S-wave is seen, and NaD lines at constant velocity are just discernible. (Center panel.) Similar, for Hα emission in CSS1055+09. (Bottom panel.) Similar, for Hα emission in CSS 2335+19.

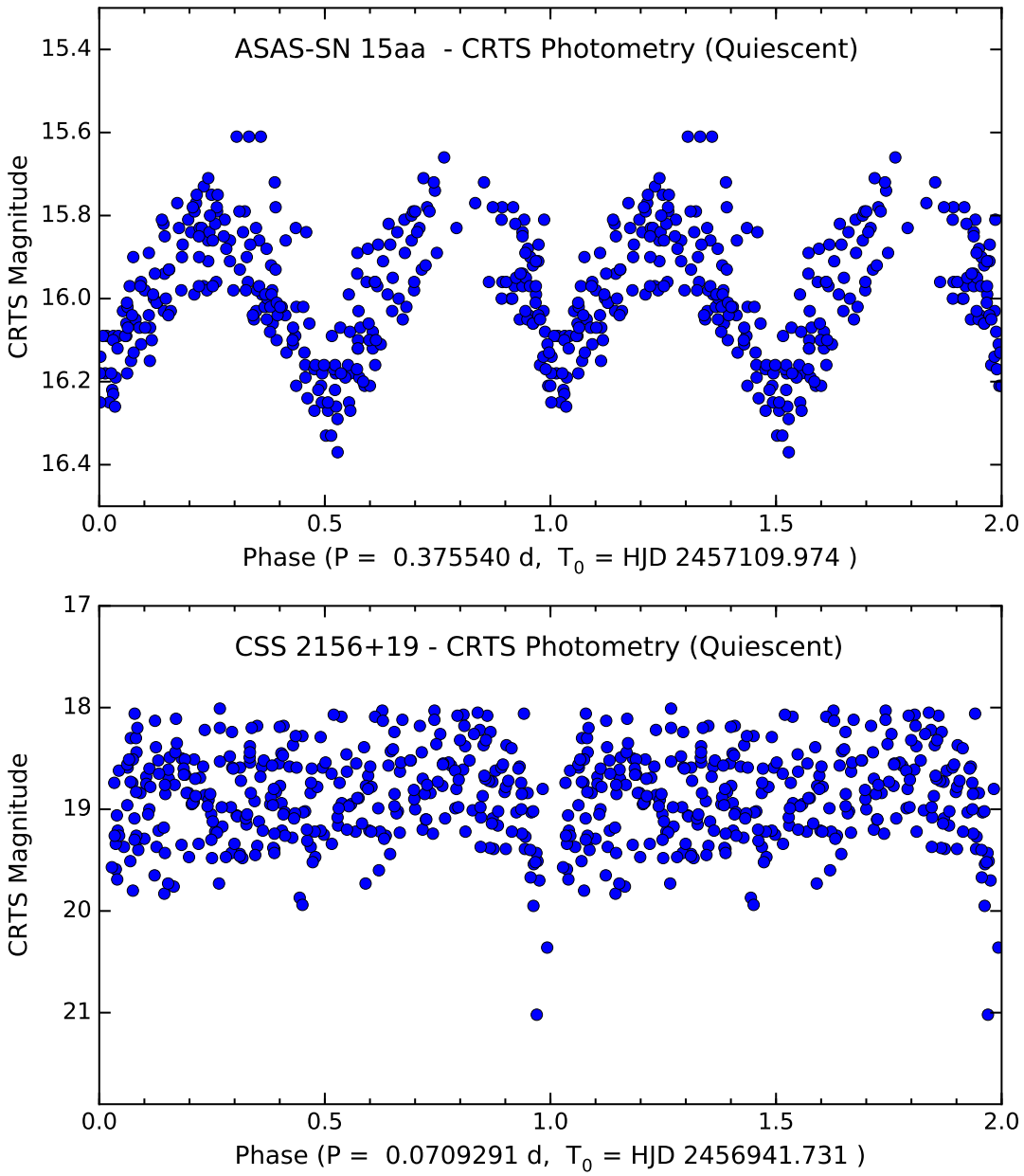

Fig. 12.— CRTS photometry of ASAS-SN 15aa (upper panel) and CSS2156+19 (lower panel) folded on candidate long-term periods. Points taken during outbursts are omitted.

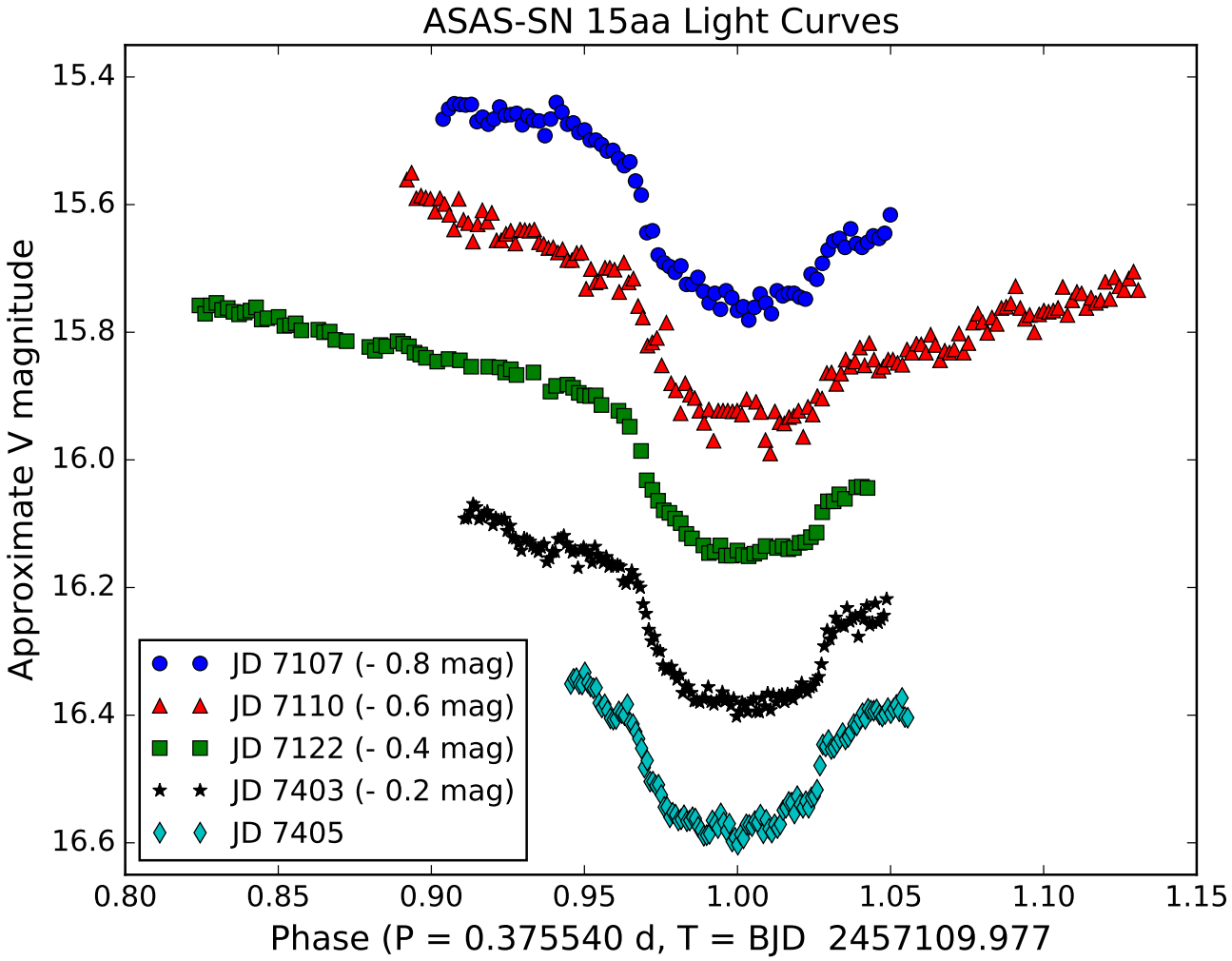

Fig. 13.— Light curves of ASAS-SN 15aa taken in 2015 March and April, and 2016 January. The horizontal axis shows the phase on the indicated ephemeris, and each night is offset by 0.2 magnitude. The vertical axis shows unfiltered differential magnitudes, scaled to rough V magnitude by adding the magnitude of the comparison star 88″ NW of the program object, at α =10:49:21.02, $\delta = -21$:46:39.6, for which APASS (Henden et al. 2015) gives $V = 16.15$. The gradual fading preceding the eclipse and the gradual brightening following the eclipse are probably due to ellipsoidal variation.

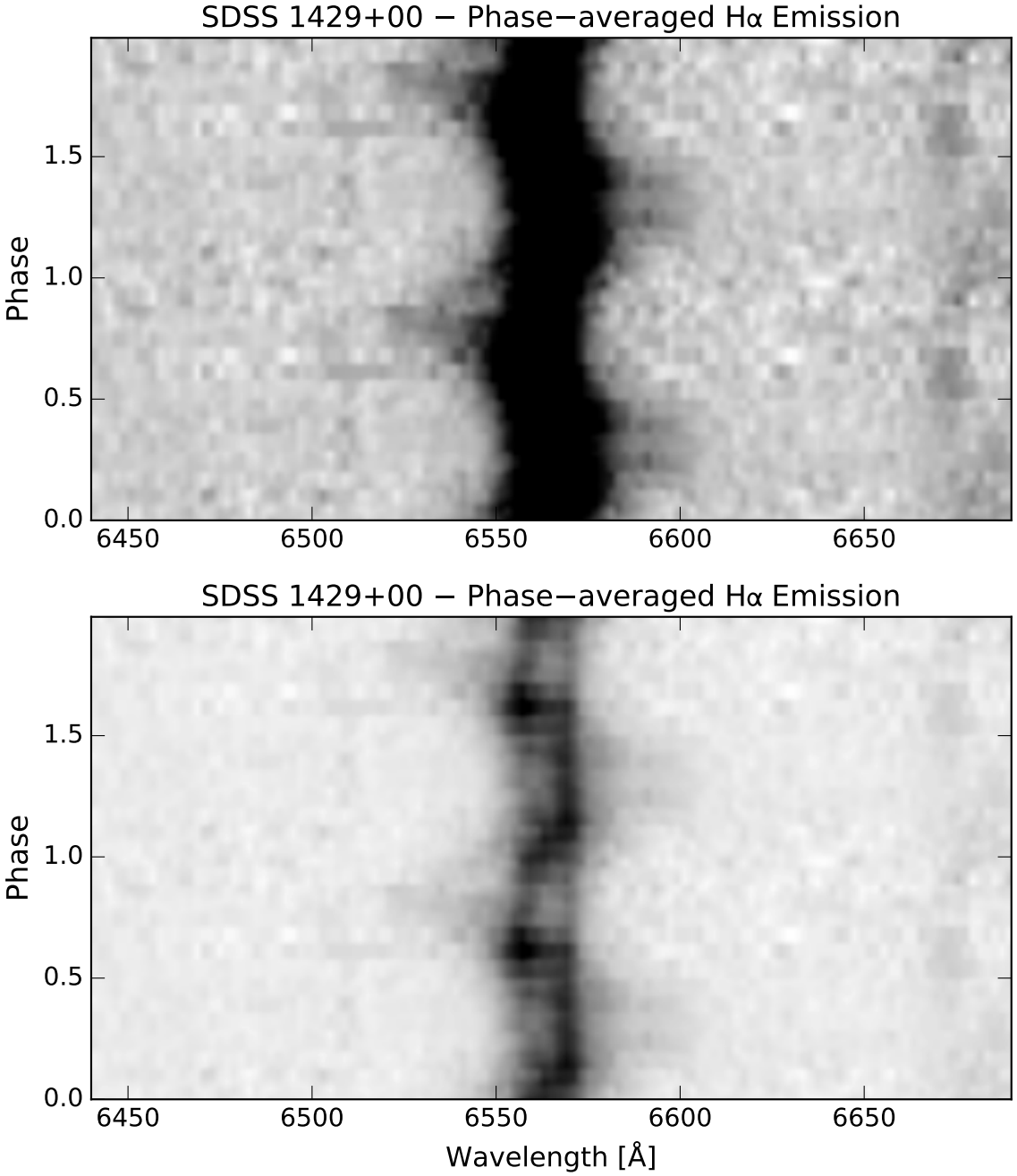

Fig. 14.— (Upper panel). Phase averaged greyscale representation of Hα in SDSS 1429+00, prepared similarly to Fig. 11. The stretch is chosen to emhpasize the high-amplitude S-wave. (Lower panel). The same data, stretched to show the line core.

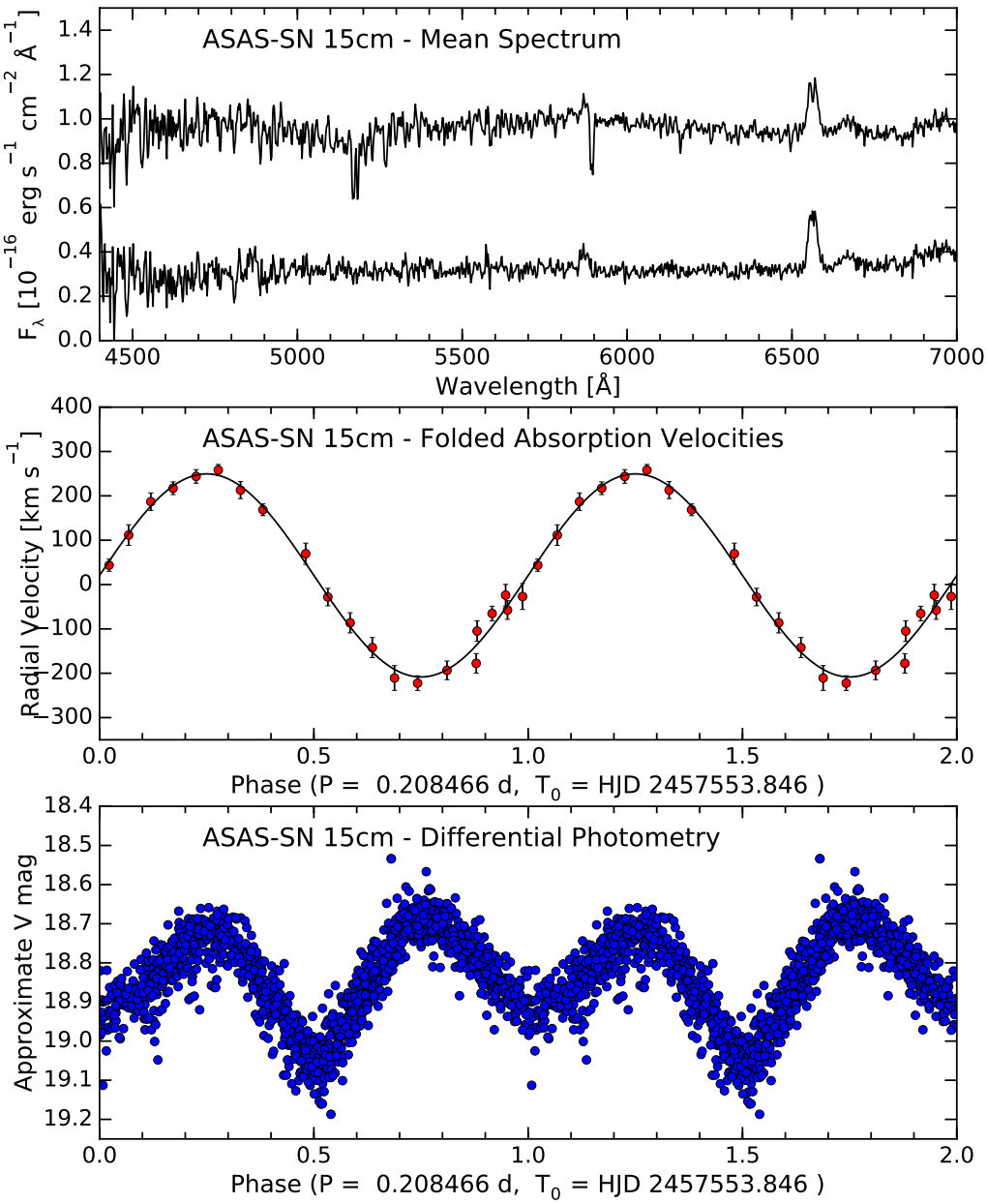
ASAS-SN 15cm - Mean Spectrum
F_λ [10^-16 erg s^-1 cm^-2 Å^-1]
Wavelength [Å]
ASAS-SN 15cm - Folded Absorption Velocities
Radial Velocity [km s^-1]
Phase (P = 0.208466 d, T_0 = HJD 2457553.846)
ASAS-SN 15cm - Differential Photometry
Approximate V mag
Phase (P = 0.208466 d, T_0 = HJD 2457553.846)

Fig. 15.— (Upper panel). Mean spectrum of ASAS-SN 15cm, formed by shifting all spectra to the velocity of the secondary star before averaging. The lower trace shows the spectrum after subtracting a spectrum of the K2V star HD101011, scaled to a synthetic $V = 19.5$. (Center panel.) Absorption-line radial velocities folded on the orbital period, with the best-fitting sinusoid (Table 3) superposed. (Lower panel.) White-light differential photometry, folded on the orbital period. The main comparison star lies 23 arcsec from the target in PA 155 degrees; its SDSS magnitudes imply $V \sim 16.1$. The vertical scale has been offset by this amount to give approximate V magnitudes.

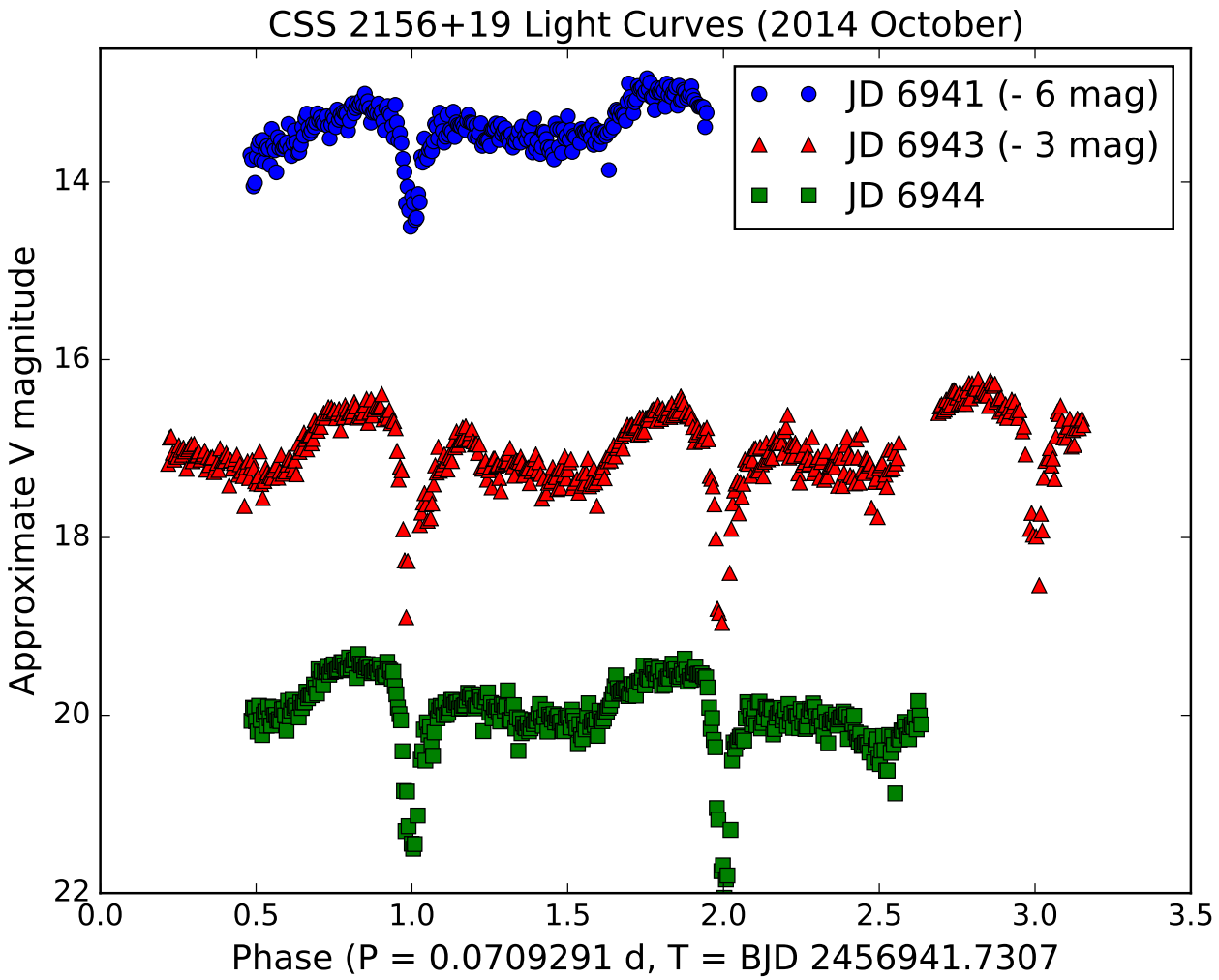

Fig. 16.— Light curves of CSS2156+19 taken on three nights in 2014 October. The horizontal axis shows phase on the indicated ephemeris, with phase increasing monotonically through each night, and nights offset by 3 magnitudes as indicated. The V magnitude used for the vertical scale is approximate, since the data were taken in white light (GG420 long-pass filter). The magnitudes are differential with respect to a star at α =21:56:38.472, δ = +19:33:17.96, for which we assumed $V = 16.18$ based on SDSS DR12.

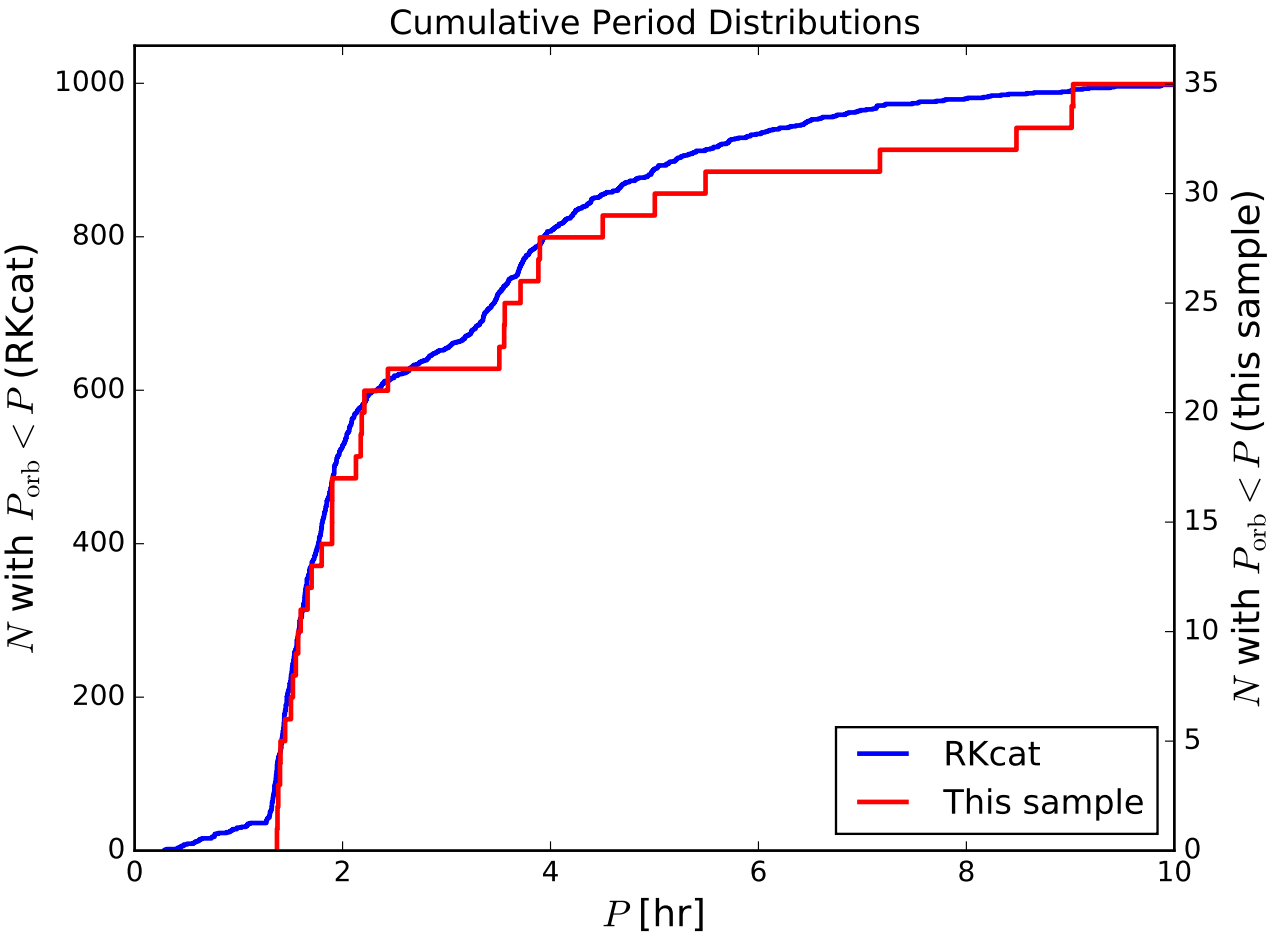

Fig. 17.— Cumulative distribution function for the present sample of 35 CVs, compared with the sample of CVs from the Ritter-Kolb catalog (restricted to $P_{\rm orb} < 10$ h).